REVIEW

www.the-innovation.org

Designing of anisotropic gradient surfaces for directional liquid transport: Fundamentals, construction, and applications

Lanlan Hou,[1,2,3] Xiaofei Liu,[1] Xinran Ge,[1] Rongjun Hu,[1,4] Zhimin Cui,[1] Nü Wang,[1,*] and Yong Zhao[1]

*Correspondence: wangn@buaa.edu.cn

Received: June 6, 2023; Accepted: September 1, 2023; Published Online: September 9, 2023; https://doi.org/10.1016/j.xinn.2023.100508

GRAPHICAL ABSTRACT

PUBLIC SUMMARY

- Non-energy consuming passive transport of liquids is studied with interest.
- Driving forces arise from asymmetric chemical, roughness, and curvature gradients.
- Anisotropic gradient surfaces show promise for a wide range of applications.
- Advanced theories and techniques need to be developed for optimized performance.

REVIEW

Designing of anisotropic gradient surfaces for directional liquid transport: Fundamentals, construction, and applications

Lanlan Hou,[1,2,3] Xiaofei Liu,[1] Xinran Ge,[1] Rongjun Hu,[1,4] Zhimin Cui,[1] Nü Wang,[1,*] and Yong Zhao[1]

[1]Key Laboratory of Bioinspired Smart Interfacial Science and Technology of Ministry of Education, Beijing Key Laboratory of Bioinspired Energy Materials and Devices, School of Chemistry, Beijing Advanced Innovation Center for Biomedical Engineering, Beihang University, Beijing 100191, China

[2]School of Printing and Packaging Engineer, Beijing Institute of Graphic Communication, Beijing 102600, China

[3]Key Laboratory of Photochemical Conversion and Optoelectronic Materials, Technical Institute of Physics and Chemistry, Chinese Academy of Sciences, Beijing 100190, China

[4]Institute of Applied Chemistry, Jiangxi Academy of Sciences, Nanchang 330096, China

*Correspondence: wangn@buaa.edu.cn

Received: June 6, 2023; Accepted: September 1, 2023; Published Online: September 9, 2023; https://doi.org/10.1016/j.xinn.2023.100508

Citation: Hou L., Liu X., Ge X., et al., (2023). Designing of anisotropic gradient surfaces for directional liquid transport: Fundamentals, construction, and applications. The Innovation **4(6)**, 100508.

Many biological surfaces are capable of transporting liquids in a directional manner without energy consumption. Inspired by nature, constructing asymmetric gradient surfaces to achieve desired droplet transport, such as a liquid diode, brings an incredibly valuable and promising area of research with a wide range of applications. Enabled by advances in nanotechnology and manufacturing techniques, biomimetics has emerged as a promising avenue for engineering various types of anisotropic material system. Over the past few decades, this approach has yielded significant progress in both fundamental understanding and practical applications. Theoretical studies revealed that the heterogeneous composition and topography mainly govern the wetting mechanisms and dynamics behavior of droplets, including the interdisciplinary aspects of materials, chemistry, and physics. In this review, we provide a concise overview of various biological surfaces that exhibit anisotropic droplet transport. We discussed the theoretical foundations and mechanisms of droplet motion on designed surfaces and reviewed recent research advances in droplet directional transport on designed plane surfaces and Janus membranes. Such liquid-diode materials yield diverse promising applications, involving droplet collection, liquid separation and delivery, functional textiles, and biomedical applications. We also discuss the recent challenges and ongoing approaches to enhance the functionality and application performance of anisotropic materials.

INTRODUCTION

Non-energy-consuming controlled passive transport of liquids over asymmetric surfaces has gained significant attention and become an important research hotspot.[1] The material systems that allow the spontaneous flow/penetration of liquid in only one direction are described as liquid diodes, which attract scientific and application interests in diverse fields such as liquid separation, water collection, digital microfluids[2] (enable fluidic functions at microscale for merging, splitting, transporting, mixing, and incubating, which makes them ideal for numerous biological and chemical platforms), energy, interface catalysis, and smart fabrics.[3–8] The anisotropic motion of droplets on a solid substrate was first observed by Greenspan in 1978.[9] The author pointed out that droplets tend to creep in a direction of greater adherence (lower contact angle) while retracting from weaker attachment regions (higher contact angle) because of the forces at the fluid/solid contact line. This work demonstrated that the surface energy gradient (chemical gradient) governs the typical behavior of droplets moving toward more wettable regions. Since then, droplet movement governed by anisotropic wettable surfaces has been extensively studied by various methods, such as electrochemistry, chemical vapor deposition, photolithography, and three-dimensional printing.[10–17] However, precise regulation of surface energy and designing of slopes are strictly required to overcome the effect of contact line pinning and hysteresis, which usually limits the movement of droplets.[18,19] In addition, the current available wettability gradient is difficult to implement over long distances due to the limited tunability of surface chemical composition and stability.

Many natural creature surfaces possess the ability of directional water transport, which provided inspiration to humans, such as desert beetles,[20,21] spider silks,[22] cactus thorns,[23,24] *Nepenthes* peristome,[25,26] and *Sarracenia* trichome.[27] The evolution of these specific surfaces was accomplished through meticulous design of hierarchical micro/nanoscale structures and chemical compositions. The topological features hold significant potential for advancing the study of liquid-diode materials through structural gradient construction. This work summarizes that self-propelled droplet motions can be considered to rely primarily on three driving forces: asymmetric chemical gradient, roughness gradient, and curvature gradient. The generation of driving forces is mainly attributed to materials morphology of scales, orientation, periodic arrangement, shape, curvatures, as well as composition properties, which affect the droplet wetting preferences and motion tendencies.[28]

In 2008, Yang and co-authors reported that droplet contact angle gradually decreased with an increasing pattern density of the microstructure.[29] They suggested that the droplet movement can be attributed to the difference between the higher and lower wetting state. This finding was further supported by Quérér et al. in 2009, who demonstrated droplet transfer toward regions of high texture density on hydrophobic pillar substrates, suggesting the role of roughness gradients.[30] To actively generate roughness gradient surfaces, researchers have designed arrayed asymmetric micro/nanopillars or ratchets with different densities and bending angles. Droplets on such surfaces preferentially move from areas of lower roughness to areas of higher roughness. The curvature gradient, which arises on asymmetrically shaped substrates, such as conical fibers found on cactus spines, and conical tubes such as shorebird beaks, provided examples of curvature gradients with both convex and concave types. In 2004, Quérér et al. studied the dynamics of a droplet on a horizontal conical fiber. They pointed out that the wettable drop spontaneously moves toward the region of lower curvature.[31] The driving force for droplets on surfaces with curvature gradients arises from the Laplace pressure gradient of the droplet. The Laplace pressure is the differential pressure between the inside and outside of a curved surface, which propels the movement of droplets with asymmetric shapes.

Currently, the field of liquid-diode materials is very active due to novel preparation methods and advanced technologies. Driven by innovative applications, scientists in this field are working on the transition from fundamental to applied research. The combination of active chemical, physical, and geometrical gradients has sparked innovative advances in droplet transport, increasing flexibility, controllability, and speed for a wide range of applications.[32–36] This article describes recent achievements in controllable liquid transport on asymmetric two-dimensional (2D) substrates, including two models for droplet sliding and spreading, as well as anisotropic liquid penetration through three-dimensional (3D) Janus membranes. This study also highlights significant advances in the practical applications of liquid-diode materials in several fields, including liquid collection and separation, cargo delivery, bioanalysis, solar-driven water purification, and functional textiles. These materials offer a convenient, eco-friendly, and energy-efficient approach to interdisciplinary research and development.

ANISOTROPIC NATURAL BIOLOGICAL SURFACES

Learning from nature, we have gained valuable insights into the remarkable capabilities in droplet transport.[37–39] Spider silk, with exceptional mechanical and chemical properties, is often observed covered with crystal water droplets in the morning, creating a beautiful sight (Figure 1A).[22] When spider silk encounters moisture, it undergoes wet reconstruction, which creates a periodic structure of spindle-knot and joint alternation, which causes a surface-energy gradient and a curvature gradient, resulting in a Laplace pressure differential. As a result, water condenses, coalesces, and transports continuously in the direction from joint to spindle-knot, exhibiting superior water collection capabilities of the spider silk. Obtaining water from air, especially in arid desert, is particularly vital for many natural organisms. Cacti have a perfect water utilization system that enables

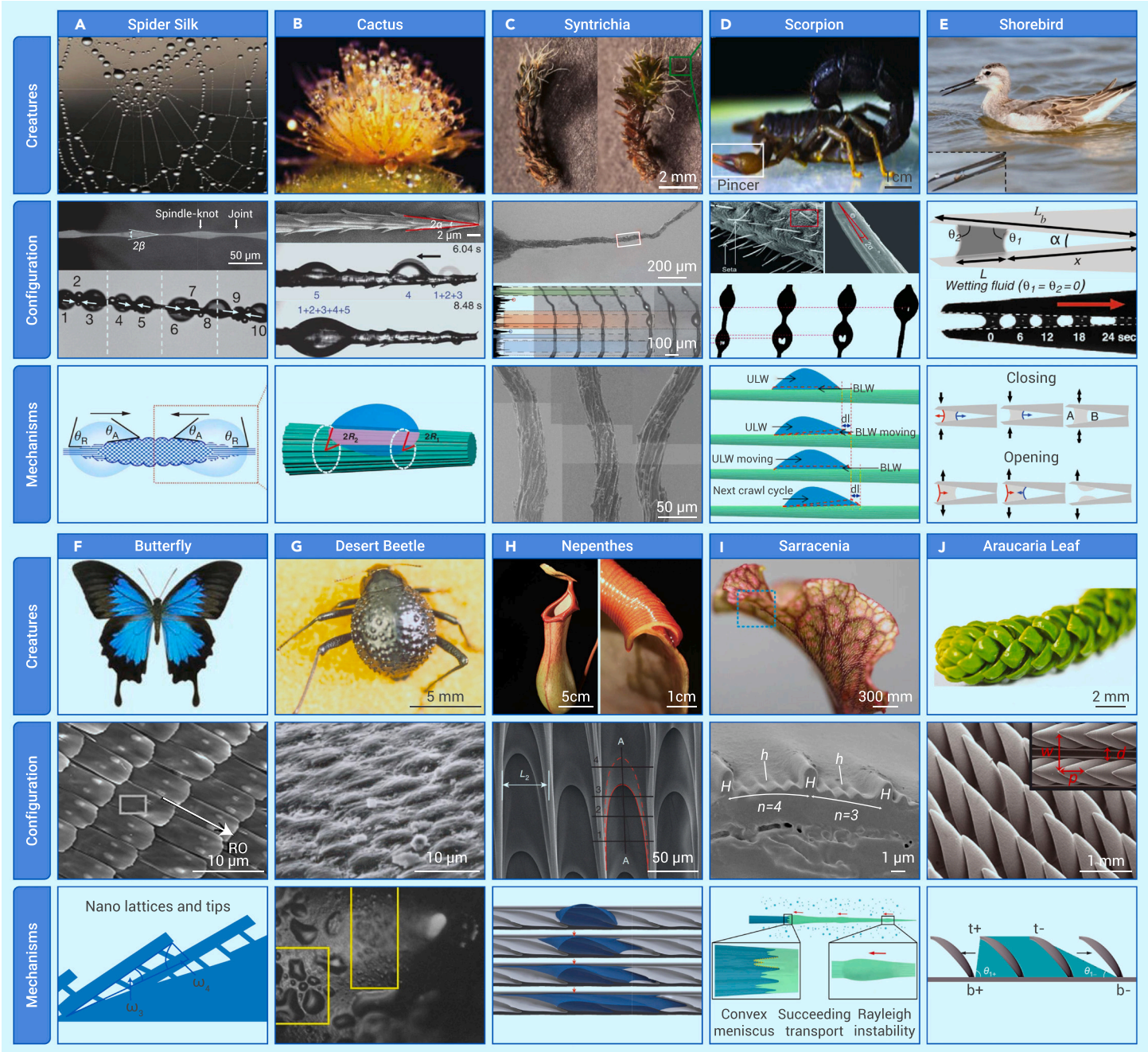

Figure 1. Liquid-diode systems in nature (A) The water droplets condense and move from the joint to spindle-knot part on the spider silk.[22] (B) The water droplets move from the tip to the bottom under the surface free-energy gradient and the Laplace pressure gradient on the needle-like spines under the asymmetric structure.[23] (C) The water droplet nucleates, grows, transports from the hair to the leaf, and is absorbed by the mosses.[40] (D) The fog capture process on the gradient conical-shaped setae of desert scorpion.[41] (E) The shorebird is capable of capturing water through its beak of concave curvature gradient structure by opening and closing the beak repeatedly.[42] (F) The water droplets can slip off the wings easily toward the outside direction on the butterfly wings and be pinned in the opposite direction.[43,44] (G) The fog collection of Namib desert beetle through its patterned non-waxy hydrophilic peak regions and wax-coated hydrophobic valley regions.[20] The valley region (left) and the peak region (right) are marked with yellow boxes, respectively.[45] (H) The water droplets move from the inner side to the outer side on the peristome of *Nepenthes* continuously and spontaneously.[25] (I) The *Sarracenia* possesses ultrafast water collection and transportation ability ascribed to the two-ordered ribs hierarchical microchannels aligned along its conical trichomes.[27] (J) Well-controlled liquid directional transport on *Araucaria* leaf consists of periodically arranged ratchets tilting toward the leaf tip.[46]

them to survive in arid deserts. The cacti's short spines can greatly reduce water evaporation and loss. Researchers have further revealed that there are well-distributed clusters of needle-like spines and trichomes on cactus stems (Figure 1B).[23] There is a hierarchical distribution of gradient grooves from a wide top to a narrow bottom, with sharp corners and oriented barbs at the tip position and belt-like trichomes at the bottom. When tiny water droplets initially deposit on the barbs, they condense into larger droplets, then directional move from the tip to the bottom trichomes, which is forced by surface-energy gradient and Laplace pressure gradient, due to the gradient grooves and asymmetric surface structure. *Syntrichia caninervis* is a widespread moss species in desert environments. This moss has developed a remarkable function to collect water efficiently, which is enabled by its hierarchical structure (Figure 1C, dry and rehydrated state).[40] Scanning electron microscopy (SEM) revealed both grooves and small barbs on its tiny hair (awn). The initial nucleation appears in nanogrooves located within a microgroove or a shallow cavity, and further growth takes place in regions with a high barb density. Subsequently, the water is transported from the base of the hair to the leaf, where it is absorbed. Figure 1D shows a desert scorpion named *Parabuthus transvaalicus*.[41] It has countless gradient conical-shaped setae that consists of parallel channels and ridges as marked by a red box distributed on its pincer. Setae are the microscale hair-like structures present on the body of insects or small animals. The scorpion seta can be easily wetted by fog, forming a hydrodynamically lubricating water film. This film

reduces interfacial resistance and facilitates accelerated droplet transfer in sliding mode. The figures illustrates the initial wetting of setae by small fog droplets, where the upper layer water (ULW) is driven by the boundary layer water (BLW) in crawl mode due to Laplace pressure difference and surface-energy gradient. Shorebirds can capture water efficiently utilizing a concave curvature gradient structure in their beaks due to the capillary ratchet-like beaks (Figure 1E).[42] This concave curvature generates a Laplace pressure gradient, enabling the stepwise ratcheting movement of a wetting droplet from the bird's beak tip to its mouth. In the competitive dynamics, the contact lines of the droplet at the leading edge and trailing edge of the bird's beak move forward and backward during each cycle of opening and closing, and finally results in a net moving inward because of the asymmetric wedge geometry.

Butterfly wings possess hydrophobic surface with anisotropic alignment micro/nanoscale roughness, giving them excellent droplet repellent properties in both static and vibrating states (Figure 1F). SEM image shows the ratchet-like overlapped scales that distributed asymmetric ridges on the butterfly wings along its radial outward (RO) direction,[43] and the positive direction tilt angle (ω) along the RO direction is smaller than the reverse direction angle against the RO direction (ω').[44] Thus, the droplets can slip off easily in the RO direction and be pinned to the opposite direction regardless of the placement angle. The severe water shortage in extreme-drought desert areas forces the local species to evolve special adaptive structures and behaviors. The Namib desert beetle's surface is composed of patterned non-waxy hydrophilic peak regions and wax-coated hydrophobic valley regions (Figure 1G).[20] During the night, the beetle tilts its body to face the airflow; tiny droplets nucleate, aggregate, and generate large droplets at the hydrophilic peaks. Once the water droplets grow beyond the hydrophilic area, they will overcome the capillary force and detach, then roll down and are transported to the beetle's mouth along the hydrophobic track under good system control, which avoids the droplets being blown away by wind. The peristome (pitcher rim) of *Nepenthes alata* features a specialized lubricated surface that enables the capture of arthropod prey through slipping and trapping mechanisms (Figure 1H).[25] This slipperiness is achieved through a delicately hierarchical micro/nanostructure that facilitates continuous and directional water transport. Periodic wedge-shaped microcavities create an asymmetric two-ordered microgroove. The asymmetric inner wedge angle in the two-level microgrooves optimizes and enhances the capillary rise in transport direction, while preventing reverse flow in the opposite direction. This slippery, anti-adhesive, and highly efficient water transport surface is expected to be of great significance in practical applications. The *Sarracenia* trichome possess special two-ordered high and low ribs, where one to five low ribs (smaller channel) are distributed between adjacent high ribs (large channel), as shown in Figure 1I.[27] Parallel microchannels induce two types of dry and wet transport models. In the dry state, the liquid transport is driven by the gradient capillary forces generated by solid-liquid contact, showing a large droplet movement model similar to spider silk or cactus spine. After wetting, the speed of liquid sliding increases significantly, forming a direct liquid-liquid contact mode. The *Araucaria* leaf has 3D ratchets with transverse and longitudinal reentrant curvatures, which enable unexpected liquid movement in and out of the surface plane (Figure 1J).[46] Liquids with low surface tension move along the ratchet-tilting direction, while liquids of high surface-tension transport in the opposite direction. Additionally, droplet rapid transport occurs on *Araucaria* leaf-inspired surfaces as a result of the pinning of the asymmetric contact line, which is caused by the transverse and longitudinal reentrant curvatures. Other organisms, such as *Phrynosoma cornutum*,[47] *Cotula fallax*,[48] *Litoria caerulea*,[49] bristlegrass,[50] wheat awns,[51] and *Stipagrostis Sabulicola*,[52] all possess specialized structures and compositions that enable water collection. In the past decades, nature has provided promising ideas for the engineering of liquid-diode materials with features of multiple compositional and structural modulation strategies. Further improved functional liquid-diode materials are expected with successful developments both in preparation and application.[53]

THEORETICAL FUNDAMENTALS

Creatures acquire water from various sources, including raindrops, mist, and ambient moisture. The underlying principles behind this process have been well studied. In this section, we illustrated the roles played by chemical gradient, roughness gradient, and curvature gradient in governing droplet transport (Figure 2).[64,65]

Chemical gradient

Chemical gradient surface has been applied to control droplet transport with a direction toward the more lyophilic (LI) side.[66–70] In 1992, Chaudhury and Whitesides first proposed a type of drop directional transport pathway caused entirely by surface chemical gradient.[54] By exposing a silicon wafer to heterogeneous decyltrichlorosilane vapor to construct a surface free-energy gradient, the water was induced to move directionally from the hydrophobic (larger contact angle) to the hydrophilic side (smaller contact angle), guided by the asymmetry forces of surface tension acting on the liquid/solid contact line.[71,72] Even on a sloping substrate surface, an uphill movement of a 1- to 2-μL water droplet can be observed for a wettability gradient surface, showing an average speed of 1–2 mm s^{-1} (Figure 2A). Under critical conditions, when the droplet size is smaller than the capillary length ($L_C = \sqrt{r/(\rho g)}$), the gravity can be neglected. The driving force can be expressed using Equation 1:

$$F_{\text{Chemical}} = \pi R_0 \gamma(\cos\theta_1 - \cos\theta_2) \quad \text{(Equation 1)}$$

Here, R_0 represents the radius of the droplet, γ is the surface tension, and θ_1 (more wettable) and θ_2 (less wettable) are the advancing contact angle and receding contact angle.[15,68,73] The direct construction of chemical wettability gradients on material surfaces are available from modification, chemical molecular adsorption,[74,75] electrowetting,[76–81] photoisomerization switchable surfaces,[82,83] and thermocapillary actuation of droplets.[84–86] Advances on chemical gradient surface can be achieved by manipulating the density of hydrophobic regions relative to hydrophilic regions.[29] Patterned surfaces of hydrophobic silicon nanopillars and hydrophilic silicon dioxide (SiO_2) stripe structures are shown in Figure 2B. The driving force varies with the proportion of superhydrophobic to hydrophilic region. Droplets show a velocity of 75 mm s^{-1} with distance of 5.2 mm (the ratio of stripe length to droplet radius was 0.83), and 46 mm s^{-1} with distance of 3.2 mm (ratio of 2.5).[55] The driving force, hysteresis, and viscosity together contribute to determine the droplet movement speed.[87,88] However, one limitation is the restricted inclination angle and confined differences in surface energy. Additionally, hysteresis effects, which refer to the contact line pinning, can affect the movement of droplets. Another challenge is the difficulty in controlling the movement direction. Furthermore, there is the issue of gradient degradation during long-term operation. To overcome these limitations, several strategies can be considered to improve the performance of these systems, including employing robust modification techniques such as covalent bonding and self-assembly, using novel materials such as self-healing mechanisms, as well as constructing micro/nanostructures.

Droplet self-propulsion is reportedly available on solid surfaces with a soft/hard stiffness gradient, where droplet "durotaxis" plays a key role in inducing asymmetric changes between the advancing and receding contact lines.[89,90] In this context, the term durotaxis describes the phenomenon where a passive liquid droplet is capable of "sensing" the stiffness of the substrate and preferentially migrating toward softer regions, driven by physical mechanisms. As shown in Figure 2C, a droplet on a soft substrate exhibits a rippling instability and deforms the substrate, raises a ridge around the contact line, and makes the droplet apparent contact angle more wetting on the softer regions to form a lenticular-like shape. The resulting gradient in advancing and receding contact angle drives droplet motion toward the softer region of the substrate.[56] Common examples of soft solid materials include oil, gel, creams, and foams.[91] It is profitable because the stiffness gradient materials are easy to prepare at a large scale. Besides, the droplet durotaxis on soft solid substrates may help to understand the particle adsorption and study of cells adhering onto the solid surface.[92]

Roughness gradient

To arrange micro-roughness gradients precisely is another efficient strategy to guide the directional transport of fluids. Roughness gradient surfaces are usually actively generated by constructing pillars or ratchets of different densities, as well as asymmetric sub-millimeter rice leaflike grooved structures.[93–96] Surfaces with various roughness favor droplets moving directionally from lower-roughness to higher-roughness areas, which is primarily subjected to the asymmetry of the contact line (difference between the advancing contact angle θ_{Adv} and receding contact angle θ_{Rec}).[97–99] Droplets on surfaces with varied roughness experience a hysteresis resistance force, which can be expressed according to Equation 2:

$$F_{\text{Resistance}} = \pi R_0 \gamma(\cos\theta_{\text{Res}} - \cos\theta_{Adv}) \quad \text{(Equation 2)}$$

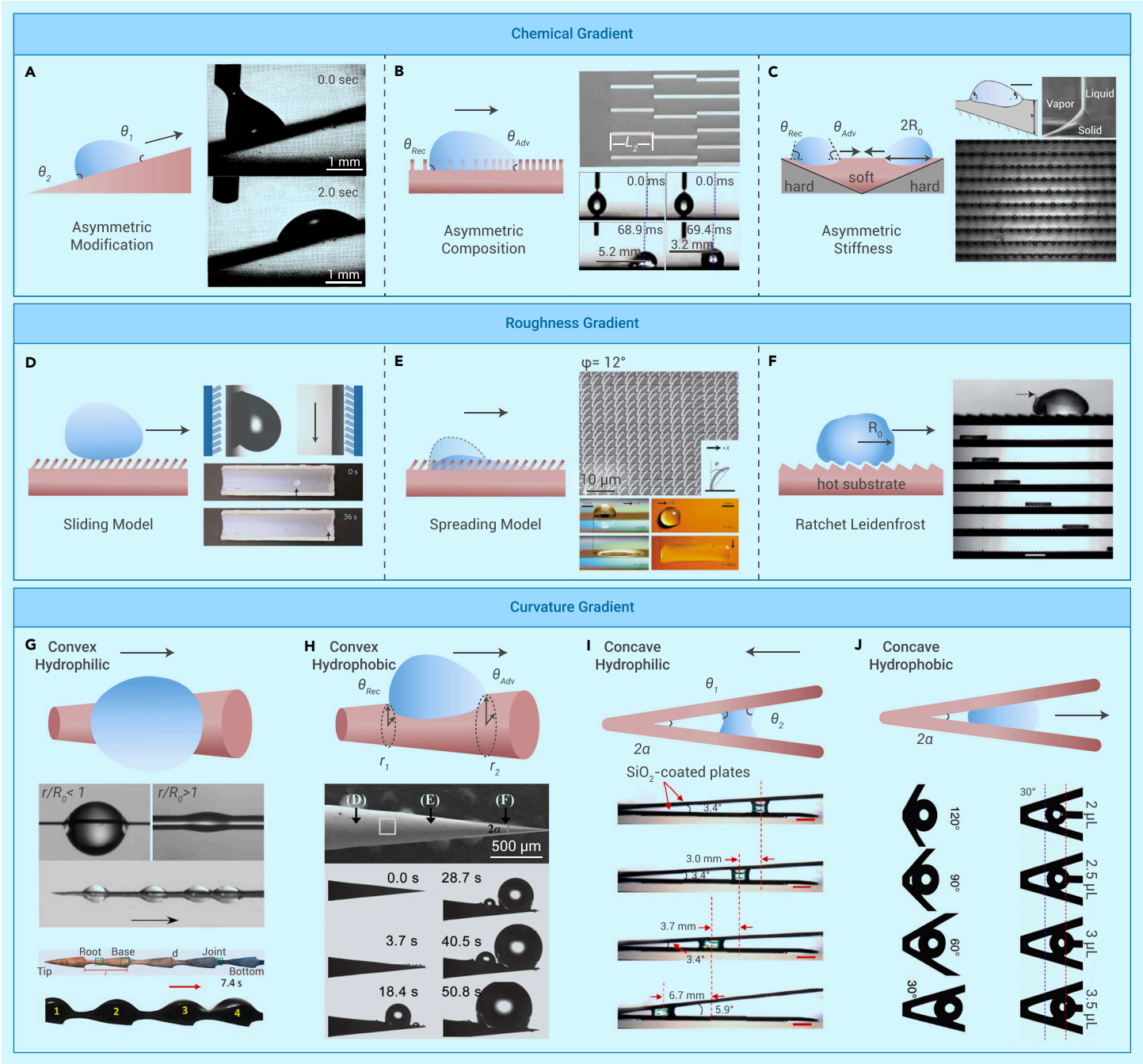

Figure 2. Droplet moving gradient driving forces The droplet moving driven by chemical gradient (A–C), roughness gradient (D–F), and curvature gradient (G–J). (A) The uphill movement of water droplet driven by surface free-energy gradient.[54] (B) The droplet transport on a patterned wettability gradient surface consisting of hydrophobic silicon nanopillars and hydrophilic silicon dioxide stripe.[55] (C) The droplet moving toward softer region on a stiffness gradient substrate because of varying of contact lines.[56] (D and E) The droplet self-propelled (D) sliding[57] and (E) spreading[58] on the roughness surface in a direction parallel to the nanostructure while pinned to other directions. (F) The self-propulsion of droplet by vapor flow escape on asymmetric ratchet Leidenfrost object.[59] (G and H) The droplet on (G) hydrophilic[31,60] and (H) hydrophobic[61] conical surface moving from large curvature (tip) to the small curvature (base) under the Laplace pressure gradient. (I) The droplet moving from the small curvature (wide end) to the large curvature (narrow end) on the hydrophilic internal surface of wedge geometry.[62] (J) The droplet transport to the wider side on the hydrophobic internal surface of wedge geometry.[63]

Technologies such as lithography,[58,100] etching,[101] replicate molding,[25] vapor deposition,[102] and 3D printing[103] provide universally accessible routes for processing various materials such as silicon wafer, polymers, and photocurable resins.

There are two modes of droplet sliding and spreading, as illustrated in Figures 2D and 2E. The sliding mode refers to the front and trailing edge of the droplet moving in one direction at the same time, while the spreading mode is the liquid's advancing contact line spreading and moving forward directionally, but the receding contact line is pinned to the original location. Figure 2D shows that tilted nanorods arrays produce anisotropic adhesive retention forces to droplets in a pin direction and release direction.[57] The droplets release and transport in the direction parallel to the nanorods' angle, while being pinned in other directions. This is because, in the release direction, the "air cushion" is confined between the droplet and the solid geometry roughness, which contributes the advancing contact line of droplet to contact the next roughness nanorods and be continuously transported. The water droplets move axially in a sliding mode on a substrate coated with an array of nanorods under external random vibration. Figure 2E shows a typical unidirectional droplet spreading with the use of an asymmetric nanostructured pillar surface deflected at 12°, which facilitates unidirectional droplet spreading of elongated-shaped droplets while being pinned to all other directions.[58] The water film front spreads ahead, and the trailing contact line stays pinned at the initial location. The simplified theoretical model revealed that the

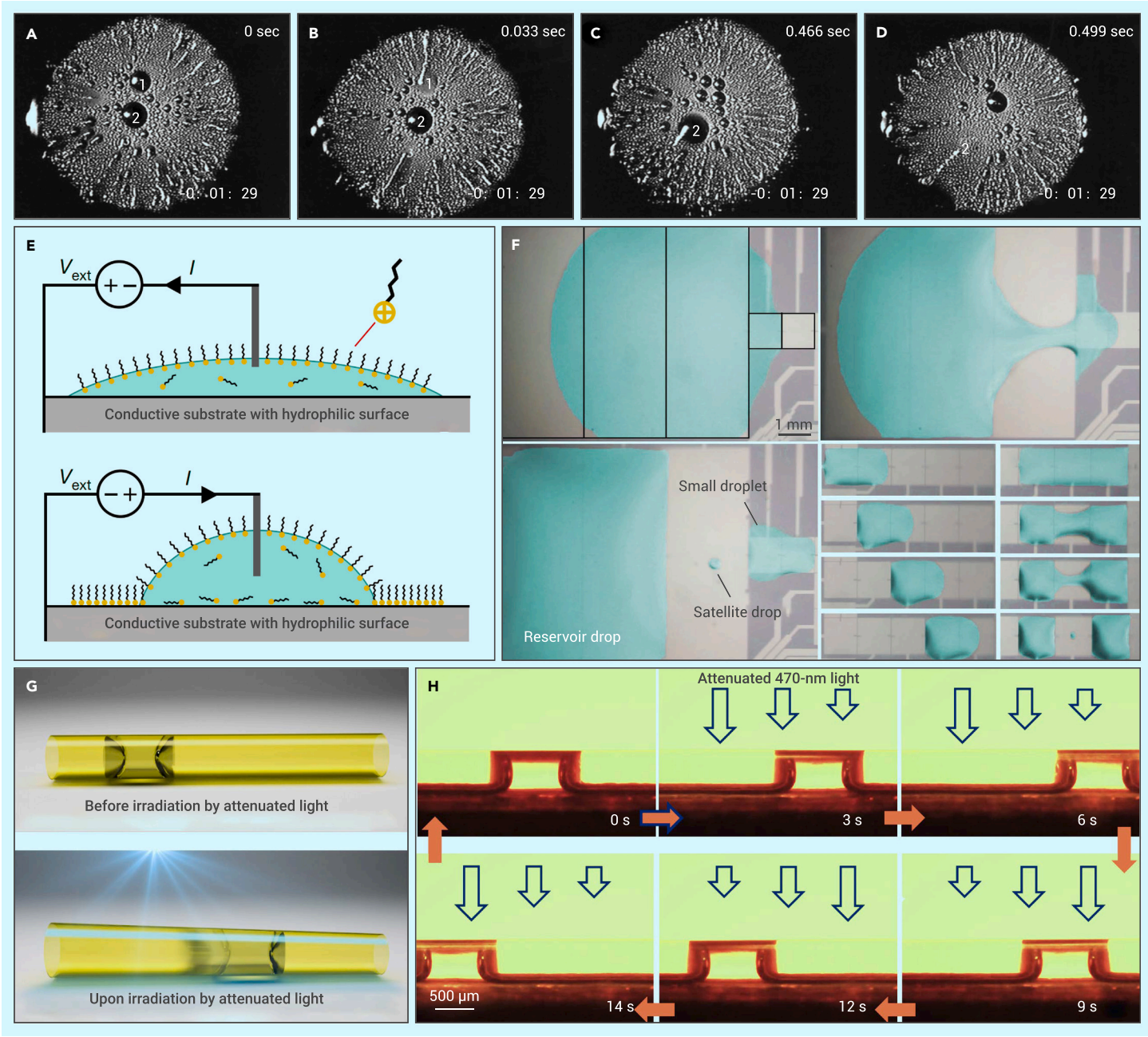

Figure 3. The droplet movement in a sliding mode (A–D) The water droplets fast movements cross the chemical wettability gradient in about 0.033 s (drop 1 and 3) and 0.47 s (drop 2).[86] (E) The adsorption of surfactant molecules on the hydrophilic conductive surface to enhance the hydrophobicity.[78] (F) The generation, transport, and splitting of water droplet driven by the surface-tension forces in the electro-dewetting process. (G and H) The wetting fluid transport inside a tube driven by curvature gradient due to photo-induced asymmetric deformation of the tube.[83]

surface wettability, nanostructure deflection degree, and the ratio of height to spacing determine the way the droplet moves, and the principle of water spreading is determined by whether the droplet front edge can propagate and reach the next nanopillar. The tunable anisotropic nanostructure roughness surfaces make the manipulations of droplets possible, which offers more controllable opportunities for microfluidic systems.

As an increasingly research topic, the droplet movements in a Leidenfrost regime at overheated surfaces are significant in the thermal management field and have been studied recently, which are related to the asymmetric ratchet morphologies.[101,102,104] A vapor film is formed when the droplet is at the Leidenfrost state over a wide range of temperature, so the liquid will not boil. In 2006, Linke et al. first reported a droplet self-propelled motion on Leidenfrost asymmetric surfaces and confirmed the active role of vapor flow in the droplet movement.[105] In 2011, Quéré et al. further promoted the droplet Leidenfrost moving.[59] The droplet was deformed by the ratchet and induced a curvature change and Laplace pressure gradient. As exhibited in Figure 2F, the droplet self-propelled in a well-defined direction, which was controlled by the vapor flow escaping under the Leidenfrost object and rectified by the asymmetric ratchet textures. Besides, the solid object of dry ice, which sublimates at atmospheric pressure, also demonstrated carrying out directional transport. The studies of topographical structures at high temperature brought in new understandings of droplet wetting dynamics and enabled the rational design of fluid control for applications.

Curvature gradient

The evolution of curvature gradient is an efficient route of biological design to ensure water collection and transport; for example, the typical spider silk, cactus thorn, and *Sarracenia* trichome can efficiently utilize the surface gradient for water collection.[106–109] Droplets on hydrophilic and hydrophobic conical-shaped surfaces tends to form barrel (Figure 2G) and clamshell (Figure 2H) conformations, respectively. The asymmetric convex curvature or concave curvature along the conical fibers creates pressure gradient on both sides of the droplet.[110–113] Laplace pressure difference has two sides, which promotes the

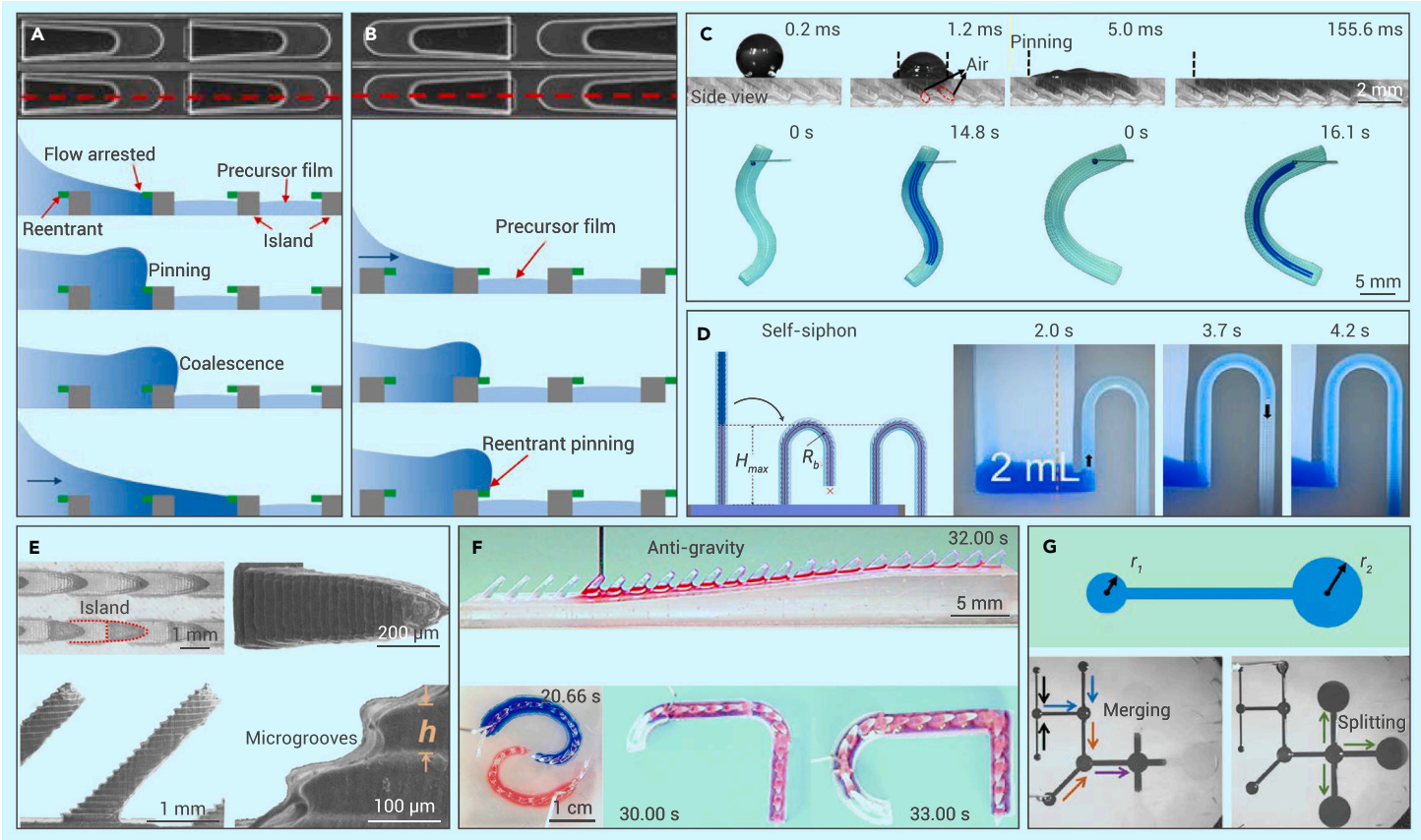

Figure 4. The droplet movement in a spreading mode (A) The water unidirectional spreading on the U-shaped island arrays with reentrant structure from the open end to the other end.[144] (B) The water was blocked in the reverse direction of the U-shaped island. (C) The well-controlled water directional transport on arbitrary designed pathways of the microcavity surface.[145] (D) The inner micro-structured bending tube to achieve the water self-siphon transport.[146] (E) The SEM images of the micro/macro dual-scale arrays by 3D printing and its applications for continuous liquid unidirectional transport.[103] (F) The liquid unidirectional transport on patterned island arrays of different microfluidics routes. (G) Directional droplet transport on designed multi-path surface caused by surface energy difference between the starting and terminal sites.[147]

condensed water droplet to move from large curvature (tip) to the small curvature (base).[114–118] The Laplace pressure $\Delta P_{curvature}$ can be expressed as in Equation 3:

$$\Delta P_{curvature} = -\int_{r_1}^{r_2} \frac{2\gamma}{(r+R_0)^2}\sin\alpha dz \qquad \text{(Equation 3)}$$

The schematic is expressed in Figure 2H, where the local mean radius of the fiber is denoted as r, l is the fiber length, α is the half-apex angle of the conical fiber, and dz is the incremental radius as a function of the position along the fiber. Thus, the driving force $F_{Laplace}$ of droplet on asymmetric-shaped surface is described in Equation 4:

$$F_{Curvature} = -\int_{l_{tip}}^{l_{base}} \gamma(\cos\theta_{Adv} - \cos\theta_{Rec})dl \qquad \text{(Equation 4)}$$

Besides water, Figure 2G illustrates a silicone droplet that is driven forward along the conical fiber surface either in a spherical shape ($r < R_0$) or in the wetting equilibrium state ($r > R_0$).[31] Figure 2H shows a droplet aggregation on the hydrophobic conical surface with a droplet growth rate of 3.27 μL s^{-1}.[61] The growth and transport of droplets are influenced by water condensation, shape, and surface wettability. According to the Kelvin equation,[119,120] the droplets with larger radius possess lower saturated vapor pressure. In the mist state, tiny droplets tend to coalesce and form small droplets, eventually merging into larger droplets. Consequently, water vapor coagulation is more likely to occur with a high radius of curvature, and, when the existing water vapor pressure exceeds the corresponding droplet saturation vapor pressure, the droplets grow rapidly. The effect of conical surface hydrophilicity/hydrophobicity on droplet collection and transport rate was investigated.[61] It has been proposed that water transport occurs more easily and rapidly on hydrophilic surfaces due to the formation of a water film. However, micrometer-sized water droplets are more likely to bounce away when colliding with liquid films than dry surfaces, which limits the droplet deposition and volume increase.[121] Conversely, the hydrophobic conical materials enable quick collection of water but result in slower water transport. This curvature-gradient-driven droplet transport on conical structures has been proposed for water collection in arid areas.[122] For example, artificial spider-silk-like fibers with periodic spindle-knots and joint structures are reported. Figure 1A illustrates how water droplets condense and move in a directed manner toward the spindle-knot. Various strategies have been developed, including dip coating,[123,124] fluid coating,[125,126] electrospinning,[127–129] and microfluidic technology.[130–132] Meanwhile, as the curvature radius of the substrate increases, the larger contact area between the liquid and the substrate results in the releasing of the total surface free energy, which can cooperate with the Laplace pressure to dominate droplet transport. The bottom insets in Figure 2G depict a systematic efficient water directional transport system achieved through an integrated tapered structure surface.[60] This system enables quick transport of droplets and facilitates rapid surface reconstruction, thereby enabling highly effective water harvest.

As for the droplet deposited inside a conical tube or cavity, the droplet self-propulsion occurs when the corner angle satisfies inequality conditions. The wedge geometry produces a Laplace pressure-gradient-driven force on the droplet; on the hydrophilic inner surface, the droplet moves from the small curvature (wide end) to the large curvature (narrow end), whereas, on the hydrophobic inner surface, it shows an opposite direction. In some cases, the liquid does not always fill the corner, considering the contact angle hysteresis. Figure 2I demonstrates droplet self-propelling by squeezing and relaxing the droplet like the shorebirds' beak opening and closing, to create a net transport flow from the trailing edge to the leading edge in three cycles.[62] When the droplet is released on the hydrophobic internal surface of a groove, the droplet movement in the opposite direction can also be observed and determined mainly by parameters of surface wettability, geometric angle, and droplet

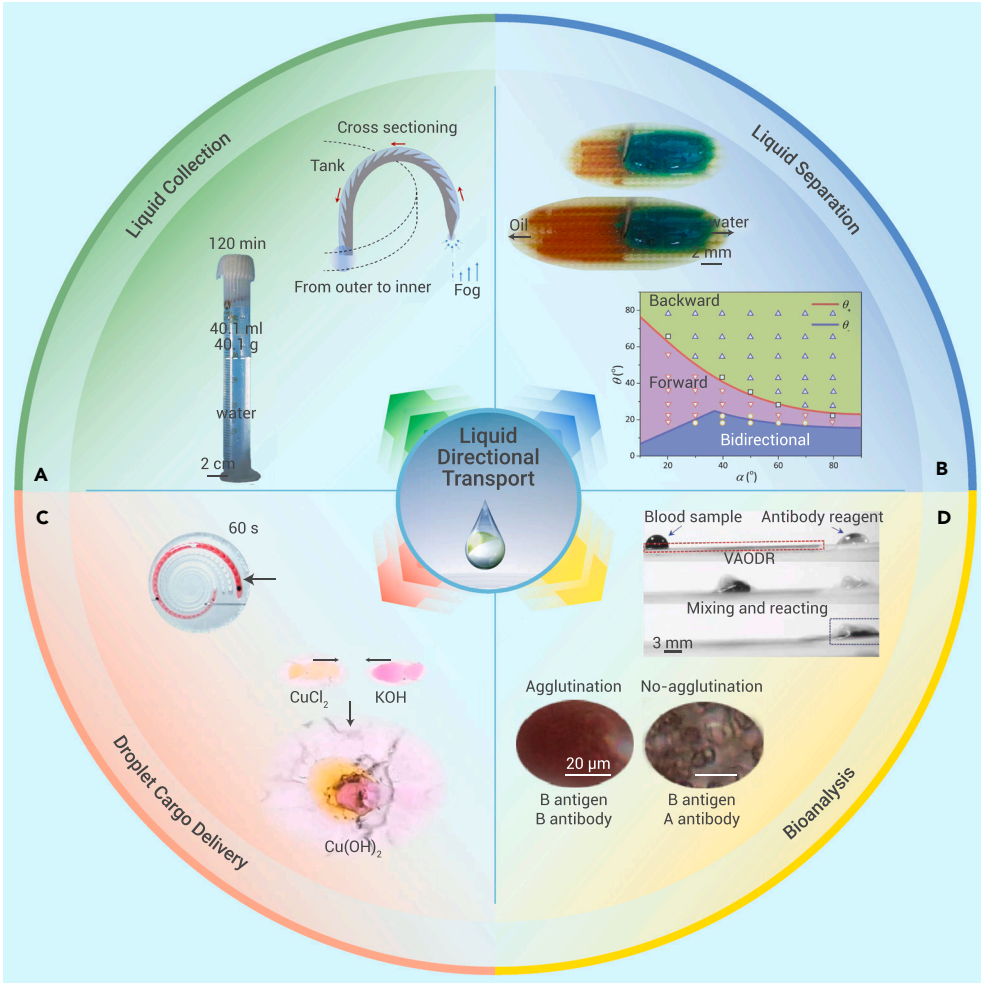

Figure 5. Applications of droplet transport on 2D plane surfaces (A) Water collection. The water condenses on the ratchet and is then transported upward to the tank and collected by an artificial collector that is composed of a peristome-mimetic surfaces.[179] (B) Oil/water mixture separation. The oil spreads along the ratchet-tilting direction (forward direction), whereas water spreads in the opposite direction (backward direction).[46] (C) Droplet cargo delivery. Controlled transport of the different liquids and micro-reactions between $CuCl_2$ solution and KOH solution.[180] (D) Bioanalysis. The biomedical detection of ABO blood-group tests.[181]

volume toward lower curvature (wide end). As illustrated in Figure 2J, the directional movement of droplets is controllable to change from an immersed state to a suspended state as the corner angle decreases (by decreasing the geometric corner from 120° to 30°).[63] As a result, the droplet will depart from the groove bottom while the volume increases.

Plants and insects ingeniously access water from raindrops, air, or other sources, utilizing their finely designed surfaces. These provided good inspiration and versatile strategies for artificial devices. The programmed operation of droplet transport has a wide range of applications, such as microfluidic, matter delivery, intelligent soft robotic, and biomedical lab-on-a-chip systems.[133] Chemical gradients, roughness gradients, and curvature gradients offer driving force to dominate directional droplets motion. The coordination of chemical composition and structure features for artificial materials led to fruitful development of biomimetic asymmetric surfaces. Advances in theory and mechanism will enable substantial advancements in the field of unidirectional passive droplet motion. High-performance fluid systems involve the utilization of chemical-, roughness-, and curvature-gradient surfaces alone or coupled, with a focus on energy conservation and environmental sustainability. The exploration of the progress and applications on designed 2D plane surfaces and 3D Janus membranes is presented in following chapters.

DROPLET MOTION ON 2D PLANE

According to the movement form of the droplet three-phase contact lines (TCLs) when the droplet moves, the directional transport of droplets on plane surfaces can be categorized into sliding mode and spreading mode. For the sliding mode, advance and recede contact lines of the droplet move forward at the same time, whereas, for the spreading mode, the front edge of droplet moves forward to show a liquid strip creeping. The droplet sliding on the slippery surface of certain infused liquids is not described here, since it is mainly controlled by applying a certain rolling angle rather than non-energetic passive transport.[134–137]

Sliding mode

The droplets' sliding movements on a plane surface are mostly induced by a chemical surface-tension gradient, while droplets spreading are generally caused by asymmetric structural gradients. In 2001, Chaudhury's group proposed an approach to guide the droplet motion by designing a cold surface with a radial surface-tension gradient,[86] where the central part of the surface shows the maximal hydrophobicity. When saturated vapor passes over the cold surface, abundant water droplets nucleate, coalescence, and grow, showing a slide movement toward the wetter direction. Figures 3A–3D show that the drops move across the gradient edge in about 0.033 s (drops 1 and 3) and 0.470 s (drop 2), powered by the droplet coalescence energies and chemical gradient forces. These transport velocities of the small drops are significantly faster, ranging from hundreds to thousands of times faster, compared to those driven by the Marangoni effect.

A common and effective way to construct a surface wettability gradient is through the use of surfactant molecular adsorption.[74,76] By electrically controlling the adsorption of surfactant molecules on a hydrophilic layer, the hydrophobicity of certain regions can be enhanced, leading to an increase of the contact angle (Figure 3E). In the electro-dewetting-governed process in Figure 3F, the droplet is governed by surface-tension forces, which facilitate its generation, transport, and splitting.[78,138] In addition, Figures 3G and 3H show a fluid self-propulsion driven by curvature gradient due to photo-induced asymmetric deformation of liquid crystal polymer tubular microactuators.[83] This strategy can be applied for various complex fluids ranging from nonpolar/polar liquid to even emulsion and liquid/solid fluid mixtures, in various types of complex paths, including straight, serpentine, Y shape, and helical shape.

Spreading mode

The droplet spreading on surfaces with asymmetric structures on precisely designed substrates was widely studied, primarily relying on the photolithography process, replication fabrication, 3D printing, and etching technology.[139,140] One common structure is the peristome-mimetic microcavity-arrayed substrate.[141,142] In this mode, the front three-phase contact point changes and a precursor film of water spreads forward and fills the microcavity induced by the topological wedge corner, while the sharp overhang structure inhibits liquid spreading in the reverse direction via strong pinning.[143]

The existence of the precursor liquid film is significant for droplet spreading. In Figure 4A, the topological surfaces are composed of periodically U-shaped island arrays with a reentrant structure in the cavity location.[144] The corner flow induces the hydraulic jump that provides a unique mechanism for liquid directional self-propulsion by overcoming the contact line pinning. The unidirectional spreading occurs in the opening side to the other side of the U-shaped island. The droplet bulk is arrested at the pinning edge, then proceeds with a hydraulic jump as the volume increases and coalesces with the precursor film. The precursor liquid film that facilitates the drop bulk undergoes the repeat process and

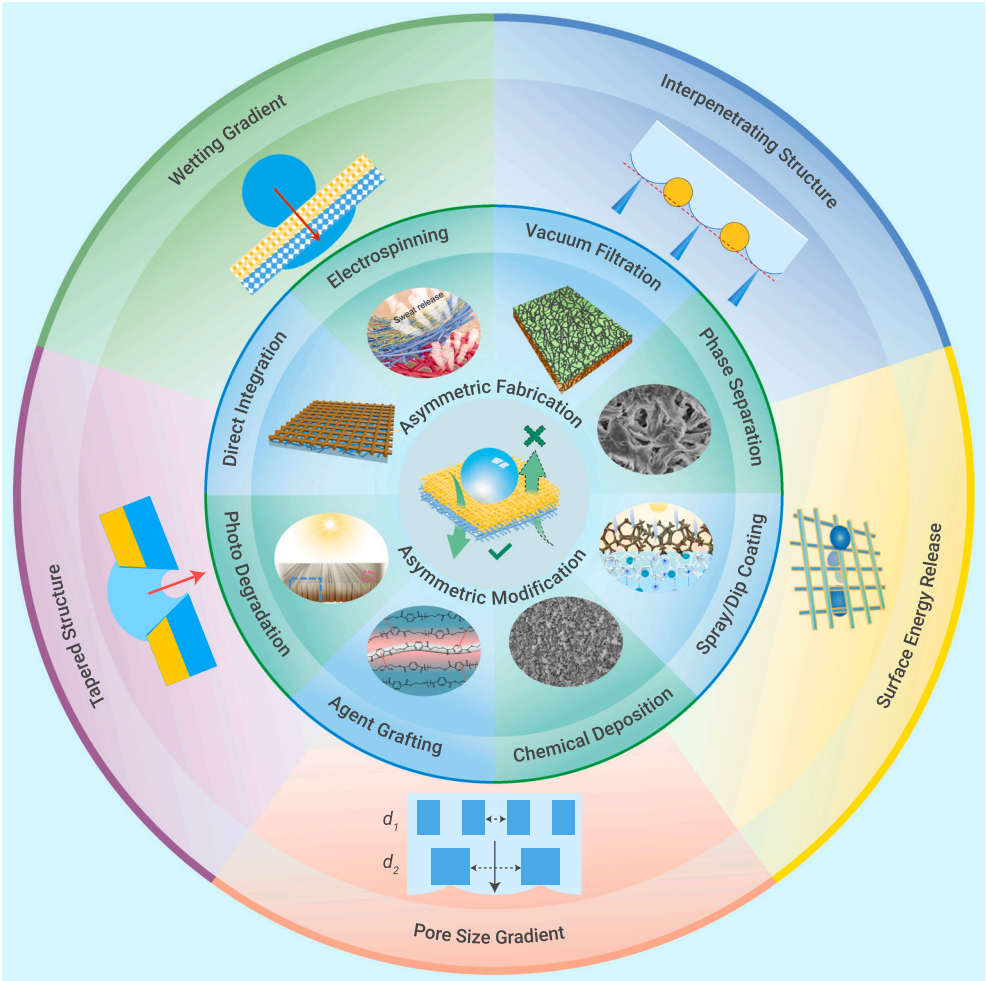

Figure 6. Outline of preparation of Janus membrane liquid-diode materials Examples of asymmetric fabrication include direct integration,[188] electrospinning,[189] vacuum filtration,[190] and phase separation.[191] Asymmetric modification involves photo degradation,[192] agent grafting,[193] chemical deposition,[194] and dip coating.[195] Types of self-propelled liquid diodes include wetting gradient, interpenetrating structure, tapered structure, pore-size gradient, and surface-energy release.

reaches the next pinning edge, resulting in continuous flow spreading without the need of an external energy input. However, the reentrant structure has its own resistance for droplet transport in the reverse direction because of the generation of an upward capillary force to restrain the liquid penetration into the cavity via pinning (Figure 4B). Owing to the directionally outward spreading of the affected drops on the hydrophilic pitcher rim, the desired liquid transport can be easily controlled to follow the designed pathways on flexible microcavity materials (Figure 4C).[145] The synergistic corner effect and topological structures enable the asymmetric spreading resistance via gradient Taylor rise. Under the cooperative effect, efficient microfluidics manipulation was achieved through a peristome-mimetic microstructure in a curvature tube (Figure 4D).[146] Water can achieve a self-siphon transport inside the bending tube. However, liquid motion faces challenges for limited handling capacity and high liquid transport speed. To achieve a rapid, long-distance, and continuous unidirectional transport, the micro/macro dual-scale arrays surface was further proposed by a simple 3D printing technology (Figure 4E).[103] The overlapped Laplace pressure leads to the anti-gravity and directional liquid transport ability (Figure 4F). A flexible microfluidic device of two liquids transported along the facile fabricated arrays showed asymmetric arc-shaped patterns, such as a tai chi symbol and other arbitrary fluid transport pathways. In addition, directional fluid transport from narrow to wide site was achieved by designing an alternating hydrophobic surface with hydrophilic transport path, which is related to the difference in surface energy between the starting and terminal sites (Figure 4G).[147] Long-distance transport on complex multiple paths can be realized by relying on the integrating, merging, and splitting of the droplets system. Moreover, this system can be applied in controllable bubbles that are transported by reversing the properties of hydrophilic and hydrophobic regions in a subaqueous environment.

However, liquid transport triggered by topography or chemical gradients generally suffers from confined transport distance, low speed, and contact line pinning effects. It has been shown that external field stimulation can improve droplet transport properties on anisotropic responsive surfaces, including electric fields (electrowetting based process, constructing charge density gradient, and electrostatic interaction),[77,80,81,148–154] light irradiation (droplet motion triggered by spatially photoirradiation-induced interface property changes),[136,155–162] magnetic field (by adding magnetic particles or by magnetic-field-induced substrate deformation),[163–169] thermal response (Marangoni effects, thermocapillary-stress-driven droplet migration, thermo-responsive surfaces),[84,101,104,156,170–175] and pH switching. Under the synergetic effect of fields stimulus and the programmable substrates, this method aims to achieve faster, long-distance, and sustainable development of self-propulsive droplet transport in specified paths.[176–178]

Applications of liquid self-propelled transport

Such liquid self-propelled directional transport on 2D plane surfaces is expected to promote practical applications in fields including water collection, liquid separation, bioanalysis, and microfluidics (Figure 5).

Water collection. The water collection process involves droplet nucleation, coalescence, growth, and transport, and rational designing on material configurations should be considered to facilitate water harvesting.[182,183] A multiscale curvatures-based *Nepenthes* mimetic structure was developed to accelerate the mist harvest and enhance the subsequent droplet transport process (Figure 5A).[179] The construction of ratchet teeth, concavities, and arch channels on the peristome surface each endows different functions for droplet collection, condensation, and transport. Moreover, comparing to traditional water-harvesting devices, this study will also benefit organic vapor-harvesting at a high speed.

Liquid separation. Liquid directional transport strategies greatly support the development of liquid-separation applications. Inspired by the dual-reentrant structure of *Araucaria* leaf, the bidirectional transport of two liquids with different surface tensions was achievable due to their specific interactions with the designed surface (Figure 5B).[46] Oily liquid unidirectionally transports in one direction while water moves in another direction, thus the oil/water can be separated. The pure oil and pure water droplets can be obtained up to nanoliters to microliters within milliseconds.[32]

Cargo delivery. Surface engineering provides a promising method for controlling the transport of droplet cargo transport at specific volumes and velocities, without requiring any energy input. Peristome-mimetic surfaces decorated with immiscible lubricant are fabricated by 3D replicating printed techniques (Figure 5C).[180] By combining surface superwettability with curvature structure, the peristome-mimetic surface is able to transport droplet cargoes with a lower surface tension compared to the lubricant phase over long distances at fast speeds. Moreover, such targeted droplet delivery systems can be applied to microreactor concepts, based on precise control over chemical composition and mobility control.[184,185]

Bioanalysis. Biomedical chips that enable precise control of tiny droplet transport are gaining popularity due to their exceptional flexibility and versatility. These chips offer significant advantages, as they eliminate the need for complex equipment and require only a small amount of sample for operation. For example, by establishing liquid-handling procedures, a slippery liquid-infused

porous surface without contact angle hysteresis and contact line pinning can be used as a bioanalysis platform and applied to the urinary stone disease metabolic workup.[34] Besides, a vibration-actuated, biocompatible, and adaptable biomedical platform was developed based on lubricant-infusion slippery ratchet arrays surface. In Figure 5D, the programmable, large-volume (0.05–2000 μL), and fast-velocity (~60 mm s^{-1}) omni-droplet transport is achieved and thus can be used for biomedical detection, including ABO blood-group tests and anticancer drugs screening.[181]

DROPLET PENETRATION ON 3D JANUS MEMBRANES

Asymmetric-wettability Janus membranes were extensively studied for their spontaneous unidirectional liquid permeation across the membrane direction as a liquid diode. Anisotropic forces exerted on droplets at asymmetric interfaces lead to unidirectional liquid penetration, ie, LI and lyophobic (LO).[186,187] Liquid could penetrate in LO to LI direction, while being intercepted in the opposite direction (Figure 6). Directional liquids transport can be controlled by adjusting the orientation of the Janus material.

Fabrication of Janus membrane

Two routes are proposed to design the wettability gradient on Janus membranes. The first is referred to as the asymmetric fabrication method, where two membranes with opposite wetting properties are integrated. The second method, refer to as the asymmetric modification method, involves selectively treating one side of a homogeneous wetted membrane to form an asymmetric wetting interface. Figure 6 summaries the outline of Janus liquid-diode materials. The asymmetric fabrication route involves direct integration,[188,196–198] asymmetric electrospinning,[120,189,199–204] vacuum filtration,[190,205–208] and phase-separation methods.[191,209,210] The asymmetric modification methods include photo degradation[192,211,212] and photo polymerization,[213] chemical grafting,[193,214,215] deposition,[194,216,217] spraying/dip/floating coating,[218–220] and laser microfabrication strategies.[221–224] Asymmetric preparation is more widely used because of its advantages in flexible regulation of material composition, wetting gradients, layer thickness, and pore size. Moreover, it offers the opportunity for multilayer liquid diodes of hierarchical asymmetric films, such as trilayered[225] and quadlayered[215] liquid-diode membranes. In addition, with the increased interest in directional liquid transport, other kinds of self-propelled liquid diodes are investigated. Studies demonstrated that droplet self-motion could be realized by the synergetic effect of interpenetrating interface structure[204] and cone hole structure,[226] or even driven by asymmetric pore-size gradient structures alone.[227] Moreover, liquid diodes could be realized by releasing surface energy on slippery surfaces.[228]

Mechanisms of Janus liquid-diode membrane

The wettability gradient guides droplet anisotropic permeation due to the movement of air/liquid/solid TCLs under asymmetric wetting forces, and, when it contacts the hydrophilic layer, it is followed by TCL rupture and then droplet penetration (Figure 7A).[199,230,231] Droplets are blocked until they reach the maximum Laplace pressure (Figure 7B). This suggests that the short distance between the LO and LI layers facilitate liquid penetration. Recently, we proposed a conceptual model of the interpenetrating LO/LI interface-structure-assisted Janus liquid diode, which proves the important effect of interface structure in accelerating droplet penetration by reducing the distance the droplet moves.[204,229] In Figure 7C, it was demonstrated that the curvature of liquid meniscus could be minimized compared to the routine contact model, and thus accelerating the liquid to contact and penetrate the hydrophilic side. This interpenetrating structure offers design options for optimal design of Janus membranes in applications. Moreover, a conical micropore enhancement mechanism on Janus liquid diode was proposed and verified.[229] The results showed the tapered large to small pore structure from the hydrophobic side to the superhydrophilic side, which contributes to faster droplet transport. It is because this that the conical structure generates minimal hydrostatic pressure in the intrusion process, maximal driving force in the wetting process, and minimal resistant force in the absorption process as indicated in Figure 7D.

In addition, researchers investigated the effect of pore-size gradient of a membrane on liquid directional transport. Janus membranes consisting of hydrophilic nanopores (II side) and superhydrophilic micropores (I side) were prepared with a controlled pore-size gradient structure.[226] Water droplets are blocked on the I surface but could be from the nano- to the micropore (II to I) side owing to the competition between spreading and penetration (Figure 7E). Moreover, by adjusting suitable pore-size gradient distributions, droplets could achieve bidirectional permeation or block both directions. Furthermore, Shou and Fan reported a diode effect attributed to the geometrical structure by integrating two hydrophilic submillimeter mesh and submicrometer membranes together.[227] The water droplet can penetrate from the larger pores on the mesh side to the smaller pores on the membrane side. During the flow from the membrane to the mesh direction, the droplet experiences a sudden expansion of the flow path, leading to the pinning of the contact line based on the Gibbs pinning condition. System energy gradient is another strategy to generate controllable droplet transport. An integrated orthogonal anisotropic slippery mesh consisting of a horizontal track (H track) and a downhill track (D track) was prepared, which water can only unidirectional penetrate from the D to H side when in a D-track-up and H-track-down model (Figure 7F).[228] By adjusting the contact area between the liquid and the substrate, the total energy of the system can be controllably modulated (Figure 7G). In the D-to-H track direction, the contact area between the droplet and the track increases and the total surface energy is successfully released to drive the droplet movement (Figure 7H).

Applications of Janus membrane

The Janus heterogeneous membrane exhibits liquid-diode effects, enabling effective management of liquid penetration in a specific direction. Numerous Janus materials have been developed, drawing inspiration from natural surfaces and leveraging advancements in nanofabrication and engineering processes. These materials have made significant progress in areas such as water collection, liquid separation, solar water purification, functional textiles, and biomedicine .

Water collection. Water collection is a process that typically involves droplet coalescence, growth, transport, and collection.[120] Inspired by the asymmetric microtopology of cactus spines and the heterogeneous hydrophobic/hydrophilic micropattern of the back of desert beetles, the Janus membranes have the function of collecting water droplets and transporting them in a directional manner from the hydrophobic side to the hydrophilic side.[218] The hydrophobic/hydrophilic Janus system for fog collection applications is shown in Figures 8A and 8B.[188] Furthermore, the released surface sites allow repeated capture of droplets, enabling continuous water collection in an energy-free and -efficient way.[192,198] Furthermore, it would be desirable to rationally design more water collection points and reduce the re-evaporation rate of collected water. Therefore, our group proposed a topology/wettability binary cooperative strategy that is composed of a hydrophilic nanoneedle layer and a hydrophobic nanofiber layer.[120] In Figures 8C and 8D, the asymmetric topology offers more distinct water collection sites; moreover, it induces a Laplace pressure difference. Besides, the alternate hydrophobicity/hydrophilicity induces a surface-energy gradient and thus synergistically improves water collection performance. The Janus materials systems show potential application in accessing water from the air in arid regions.

Liquid separation. Janus membrane are used for oil-water separation and emulsion separation, with outstanding efficiency due to their selective permeability to oil or water, typically used for filtering oil from water.[234,235] Relatively few studies reported for water filtering because the oil phase can easily contaminate the hydrophobic layer and prevent water transport. This oil unidirectional penetration of Janus membranes can generally be divided into two types: the in-air oleophilic/oleophobic membrane and underwater oleophilic/oleophobic membrane. For the in-air oleophilic/oleophobic membrane, the water is often blocked in both directions due to its in-air superhydrophobicity on both sides, while the oil is allowed to penetrate in the oleophobic to oleophilic direction and thus is separated.[236] Compared with the single-layer porous hydrophobic/oleophilic membrane, the Janus material can typically achieve higher separation flux of oil transport in an oleophobic to oleophilic direction under asymmetric wettability, because the oleophobic layer can effectively restrain the plug problems caused by oil contamination. Moreover, the underwater oleophilic/oleophobic membrane typically exhibits the ability of directional oil droplet trapping (Figures 8E and 8F).[232] Under the assistance of buoyancy, continuous selectively flowing oil separation is achieved on Janus gradient membranes, which can be used for oil recovery from industrial flowing wastewater.[216,237]

Solar water purification. Membrane desalination offers a promising approach to alleviate the global water shortage issue.[238–240] Recently, a water

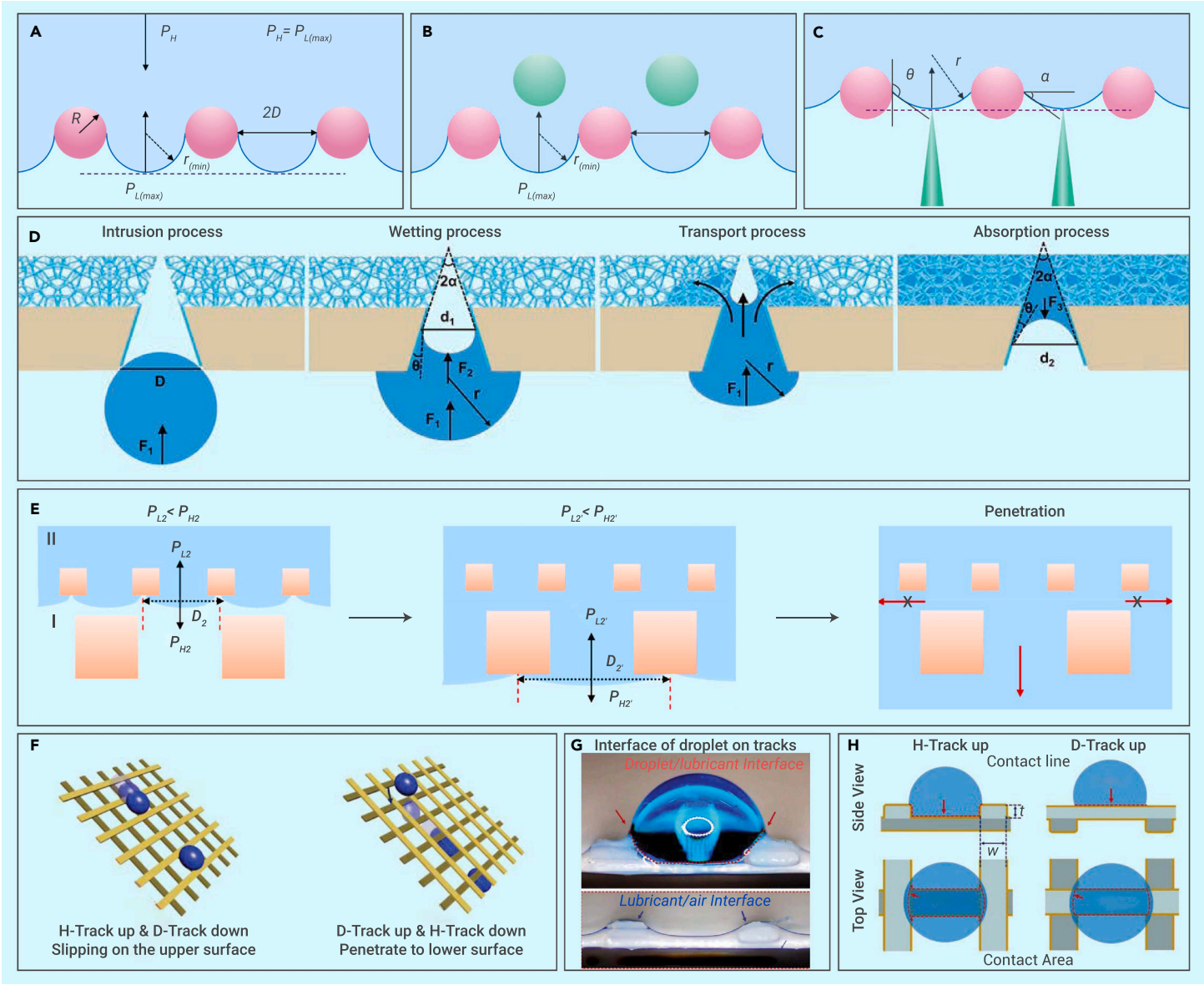

Figure 7. Mechanisms of liquid unidirectional penetration on kinds of Janus membrane (A and B) Droplet penetration in LO to LI direction while blocked in LI to LO direction on wetting gradient drives Janus membrane. (C) Interpenetrating structure enhanced Janus liquid diode.[204] (D) Conical micropore structure enhancement of Janus liquid diode.[229] (E) Pore side gradient-driven liquid diode.[226] (F–H) Liquid diode dominated by surface-energy release.[228]

purification method known as interface solar vapor generation (ISVG), based on high-performance photothermal materials, has become a hot topic because of energy-free, green and efficient, and environment-friendly features. ISVG technology uses a photothermal material at the water/air interface to absorb sunlight and generate heat. Then the converted heat is used to heat the polluted or brine water, and ultimately to obtain clean water through vapor condensation. The high-performance solar vapor system should integrate efficient light absorption, low heat loss, water supply and timely vapor diffusion, and a self-floating structure. However, single-layer hydrophilic evaporator systems suffer from significant heat loss, and, on the other hand, hydrophobic evaporator materials often encounter inadequate surface water supply.[241] It is difficult for a single-layer membrane to realize the coupling of the above multiple functions. Owing to the cooperative construction of the two membranes, Janus membrane improves the efficiency of solar to vapor conversion due to independent coupled regulation.[242,243] As shown in Figure 8G, the Janus evaporator has a hydrophobic upper photothermal layer and a hydrophilic insulation layer, which is an effective method for water desalination and inhibiting salt deposition because of sufficient interconnected channels for quickly salt dissolution due to water pumping.[233] The Janus evaporator shows stable vapor generation of 1.30 kg m^{-2} h^{-1}, and the salinity after purification is far below what is defined by World Health Organization in Figure 8H. The salt resistance due to Janus structural design helps the long-term cycling stability.[195,244] In addition, we proposed a Janus ISVG device that integrates a superhydrophilic photothermal layer and a superhydrophobic thermal localization layer (Figure 8I).[35] The high vapor production was 1.88, 3.95, and 5.65 kg m^{-2} h^{-1} under simulated 1/2/3 suns with energy input of 1/2/3 kW m^{-2} (Figure 8J). In Figure 8K, the hierarchical-structured photothermal layer can achieve broad-spectrum solar light absorption and low light reflection. The bottom insulation layer of ultra-low thermal conductivity could restrain a stable air layer underwater to prevent thermal transfer to bulk water. Meanwhile, water is self-pumped unidirectionally from bottom hydrophobic layer to upper hydrophilic layer by virtue of the anisotropic wettability. With the solar vapor conversion efficiency up to 78.56%, this synergetic strategy offers a comprehensive solution for freshwater production (Figure 8L). Additionally, Janus evaporator with additional features such as magnetic localization[245,246] and windproof and rotation resistance abilities[247] has been proposed, which allows solar water purification in complicated surroundings.

Functional textiles. Currently, there is a growing demand for quick-drying clothes. Personal moisture-management fabrics can quickly transport sweat and water vapor from the surface of human skin to the environment to achieve a quick-drying effect. These fabrics provide a comfortable wearing experience in hot and humid environments but also reduce energy consumption. Janus fabric with internal hydrophobic and external hydrophilic characteristics can induce

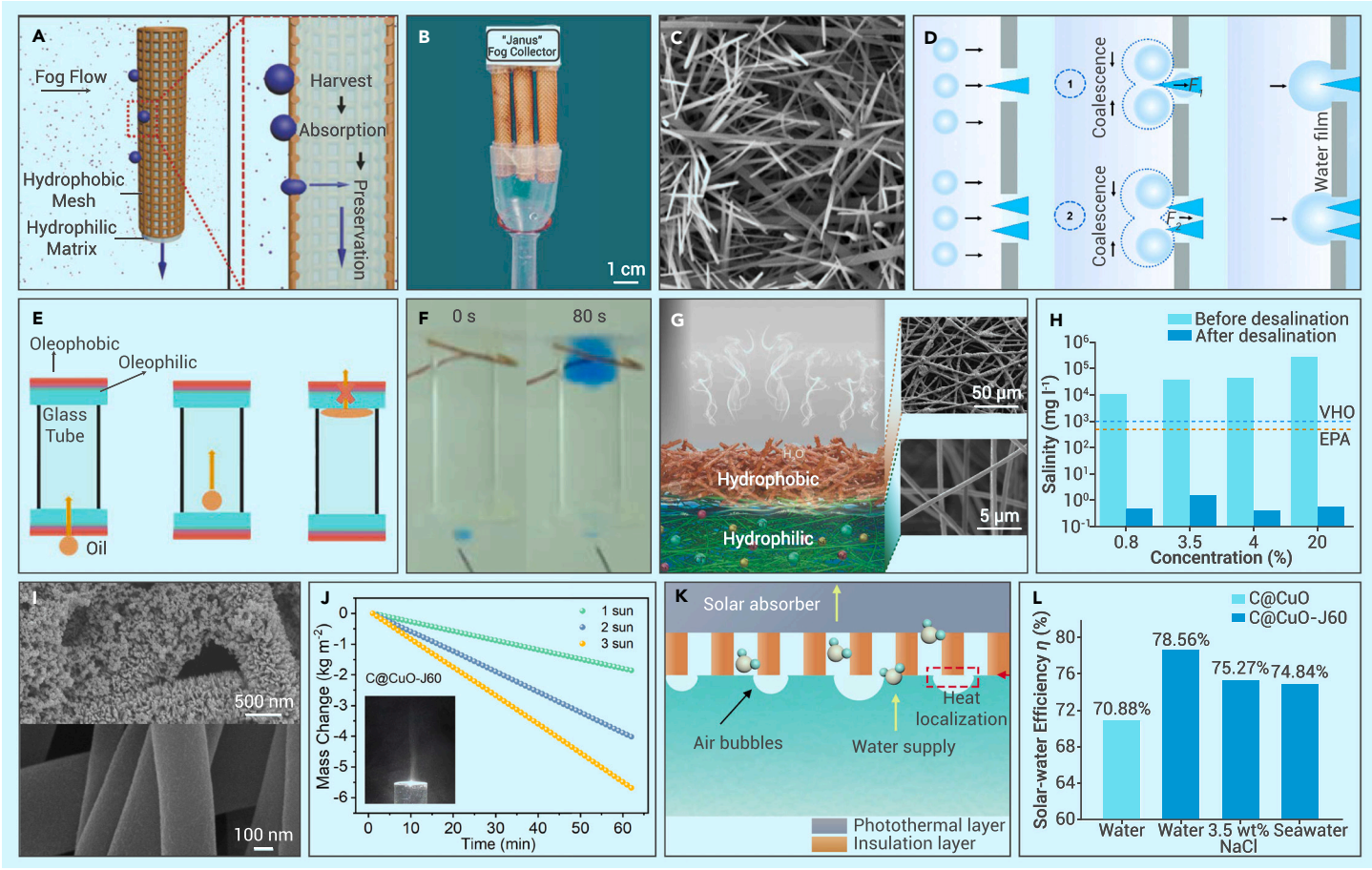

Figure 8. Applications of the Janus membrane system in water/fog collection, liquid separation, and solar-driven water purification (A and B) The hydrophobic/hydrophilic Janus system for fog collection applications.[188] (C and D) The topology/wettability binary cooperative system for droplet capture, growth, coalescence, directional transportation, and water collection.[120] (E and F) The underwater directional oil penetration and collection by the Janus membrane system.[232] (G) Hydrophobic/hydrophilic Janus evaporator demonstrates high-efficiency water purification of 1.30 kg m^{-2} h^{-1}.[233] (H) The salinity before and after desalination. (I) Hydrophilic/hydrophobic Janus membrane integrates high-performance light absorption and low thermal loss.[35] (J) The evaporation rate of the C@CuO-J60 evaporator under 1/2/3 suns of 1.88, 3.95, and 5.65 kg m^{-2} h^{-1}. (K) The synergistic mechanism of light absorption, heat confinement, and water self-pumped on the wettability gradient Janus evaporator. (L) The solar-to-water conversion efficiency of the Janus evaporator.

spontaneous outward transport of moisture mainly due to the wettability gradient, as well as capillary force effect, pore structure, and flexible tunable composites.[201,248,249] Thus, Janus fabrics exhibit outstanding moisture transport capacity compared to commercial fabrics. For example, by creating gradient wettability channels across a hydrophobic cotton fabric thickness, the asymmetric fabric demonstrates a directional liquid transport ability 15 times greater than the conventional Gore-Tex fabric.[250] Moreover, a Janus membrane with a reversible wettability gradient upon temperature change was designed, realizing adaptive human moisture and thermal management. Droplets can be transported from inner hydrophobic to outer hydrophilic side at high temperature. While at low temperatures, water is held on the inner hydrophilic surface and is prevented from being transported to the outer hydrophobic surface (Figure 9A).[251] The reversible liquid penetration is caused by the local shrinking and swelling of the fiber networks under temperature changes resulting in changes in surface energy and pore size (Figure 9B). Besides, hierarchical heterogeneous multilayer membranes exhibit an effort of enhanced moisture-wicking properties by creating progressive wettability and gradients in pore structure.[176,215] A sandwich-structured nanofiber fabric that has Janus wettability (Figure 9C) combined with outdoor radiant cooling properties (Figure 9D) was designed.[252] This textile thus has excellent personal thermal and moisture-management performances, achieving a rapid sweat evaporation rate of about 0.26 g h^{-1} and a body temperature drop of about 4.2°C (Figure 9E). With the further study of the Janus functional membranes, novel moisture-wicking fabrics with extended features are reported, such as inhibiting bacterial growth and invasion,[193] breathable synergistic triboelectric textiles,[253] and radiative cooling for heat management,[36] which has bright prospects for wearable clothing.

Biomedicine. In clinical medicine, conventional dressings fail in completely transferring biofluid from a wound, and excessive biofluid can delay wound healing or even cause infection. Here, Janus self-pumping dressings provide a new approach for wound healing by unidirectionally draining biofluid from the hydrophobic side to the hydrophilic side, effectively preventing biofluid from wetting the wound and thus accelerating the wound-healing process.[203] Compared with conventional dressings, this strategy avoids the adhesion problems caused by biofluid accumulation and secondary wound disruption caused by peeling dressings (Figure 9F). Figure 9G clearly shows the upward draining of biofluid. Results showed the formed epithelium after 14 days' healing by the Janus dressing, while no epithelium formed by the conventional dressing (Figure 9H). Moreover, it is expected to be used clinically in the next generation of wound-healing dressings. Besides, owing to the flexible tunability of the porous structure and interface properties, researchers proposed a type of functional Janus membrane of chitosan/hydroxyl apatite, which can serve as an effective scaffold for cell guidance and tissue regeneration.[254] In a model study of bone defects of a rat, the effective practical regeneration results are confirmed, which provides new opportunities for clinical medicine treatment. In addition, by virtue of the liquid-diode property, the researchers even achieved rapid removal of red blood cells from the blood. Because the membrane is integrated into the test strip, this makes it possible to monitor blood glucose in near real time and reduce blood waste.[255] Functional Janus fabrics are attracting increasing interest due to wide potential applications.

CONCLUSION

Natural creatures have evolved excellent capability in liquid transport and control, which inspired us through chemical, physical, and geometrical engineering and modulation in designing new liquid-diode materials. Smart fluid unidirectional control materials have made significant improvements in the last two decades, including theoretical foundation, progressive underlying mechanisms, and widespread application scenarios. It facilitates the development of the discipline,

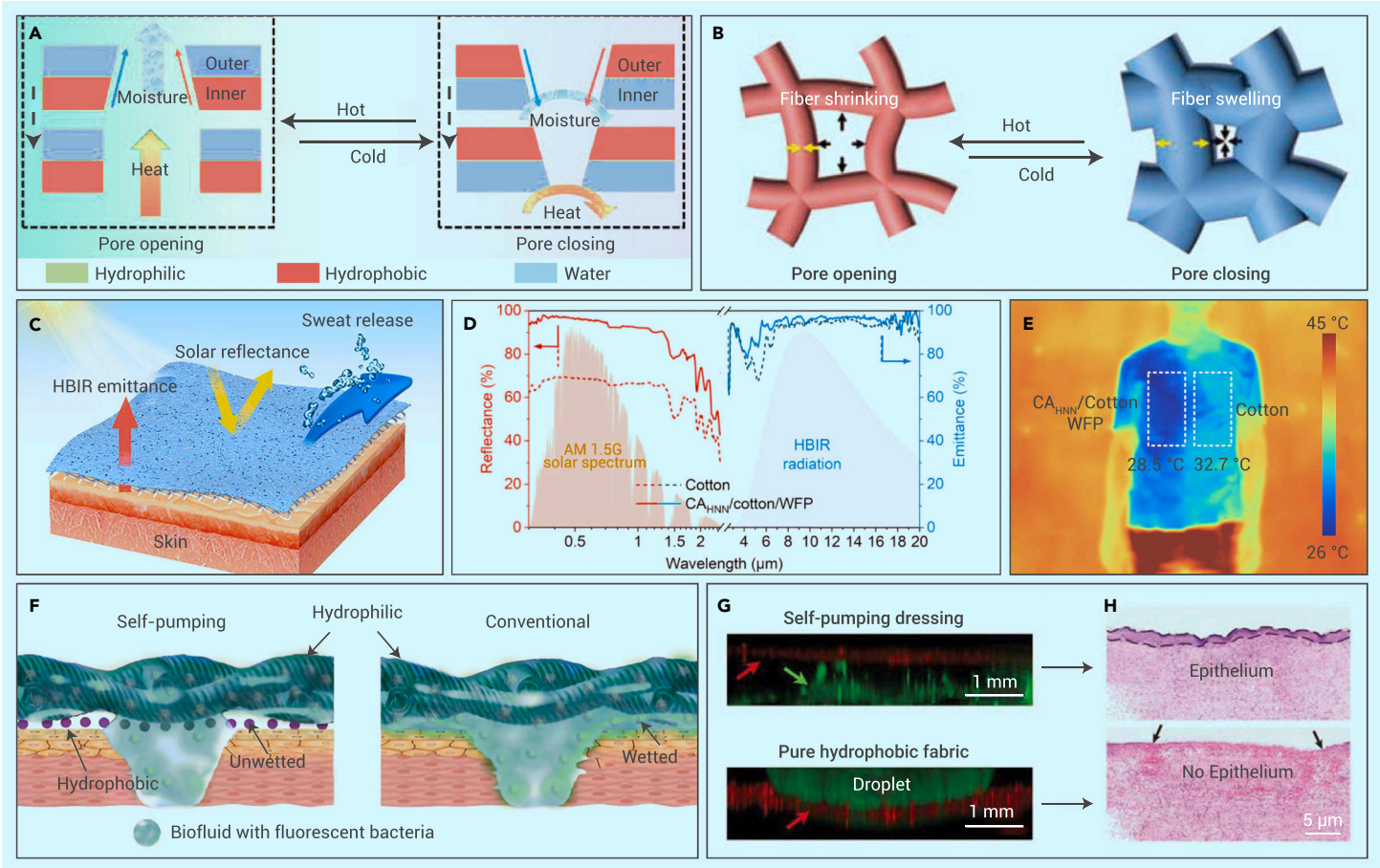

Figure 9. Janus membrane used as function textiles (A and B) The Janus membrane shows a reversible wettability gradient upon temperature change.[251] (C–E) The sandwich-structured fabric with Janus wettability used for personal thermal and moisture management.[252] (F–H) Janus self-pumping dressing accelerates the wound-healing process.[203]

digital microfluids, and functional materials. More importantly, this energy-free model contributes more in alleviating the current energy crisis. Benefitting from its unique unidirectional liquid transport behavior, liquid-diode materials show broad application prospects in liquid manipulation and separation, cargo delivery and microreactors, bioanalysis and fast response platforms, solar water purification, smart fabrics, etc. Currently, strategies and technologies need to be developed for easy fabrication, faster response speed, and long-distance liquid transport control. This development may involve robust covalent bonding, self-assembly techniques, and use of novel materials such as self-healing mechanisms, as well as hierarchical micro/nano-engineering composites. Additionally, computational simulations and predictions can be included, which will effectively mitigate risks and expedite the screening of optimum preparation conditions. Anticipated advancements in nanotechnology, bionic manufacturing, and intelligence are expected to improve the droplet control precision, materials performance, and durability. Moreover, these are likely to increase cost-effectiveness and enable large-scale preparation, thereby facilitating commercial applications. Furthermore, the role of liquid-diode materials needs to be coupled to the application scenarios for synergistic application functions. For example, as a microreactor, it requires precise fluid control, fast response, and repeatability. As a wound dressing, it also needs good breathability, sterilization and anti-inflammation properties, and to be skin friendly. Most importantly, the guiding theoretical research of chemical composition, structure, and material performances requires refined development. This includes in-depth discussions and designs that encompass chemical gradients, roughness gradients, and curvature gradients to enhance the overall performance. The fostering of synergy between theoretical innovation, fabrication technology, and application-driven approaches creates a supportive and mutually reinforcing environment. There are both opportunities and challenges associated with liquid-diode materials. The field of bionic liquid-diode materials represents a multidisciplinary and innovative intersection of research. Through collaborative efforts, it is expected that liquid-diode materials will witness promising advancements and applications.

REFERENCES

1. Bain, C.D., Burnett-Hall, G.D., and Montgomerie, R.R. (1994). Rapid motion of liquid drops. Nature ***372***, 414–415.
2. Holmes, H.R., and Böhringer, K.F. (2015). Transporting droplets through surface anisotropy. Microsyst. Nanoeng. ***1***, 15022.
3. Jing, X., Si, W., Sun, J., et al. (2022). Wettability and Droplet Directional Spread Investigation of Crescent Array Surface Inspired by Slippery Zone of Nepenthes. Adv. Mater. Interfac. ***9***, 2101231.
4. Tenjimbayashi, M., and Manabe, K. (2022). A review on control of droplet motion based on wettability modulation: principles, design strategies, recent progress, and applications. Sci. Technol. Adv. Mater. ***23***, 473–497.
5. Zhou, Y., Zu, J., and Liu, J. (2022). Programmable intelligent liquid matter: material, science and technology. J. Micromech. Microeng. ***32***, 103001.
6. Zhou, S., Jiang, L., and Dong, Z. (2023). Overflow Control for Sustainable Development by Superwetting Surface with Biomimetic Structure. Chem. Rev. ***123***, 2276–2310.
7. Pizarro, A.D., Berli, C.L.A., Soler-Illia, G.J.A.A., and Bellino, M.G. (2022). Droplets in underlying chemical communication recreate cell interaction behaviors. Nat. Commun. ***13***, 3047.
8. Charmet, J., Arosio, P., and Knowles, T.P.J. (2018). Microfluidics for Protein Biophysics. J. Mol. Biol. ***430***, 565–580.
9. Greenspan, H.P. (1978). On the motion of a small viscous droplet that wets a surface. J. Theor. Biol. ***70***, 125–134.
10. Si, Y., Dong, Z., and Jiang, L. (2018). Bioinspired Designs of Superhydrophobic and Superhydrophilic Materials. ACS Cent. Sci. ***4***, 1102–1112.
11. Villegas, M., Zhang, Y., Abu Jarad, N., et al. (2019). Liquid-Infused Surfaces: A Review of Theory, Design, and Applications. ACS Nano ***13***, 8517–8536.
12. Chen, Y., Meng, J., Gu, Z., et al. (2020). Bioinspired Multiscale Wet Adhesive Surfaces: Structures and Controlled Adhesion. Adv. Funct. Mater. ***30***, 1905287.
13. Han, K., Wang, Z., Han, X., et al. (2022). Active Manipulation of Functional Droplets on Slippery Surface. Adv. Funct. Mater. ***32***, 2207738.
14. Zhao, Z., Li, C., Dong, Z., et al. (2019). Adaptive Superamphiphilic Organohydrogels with Reconfigurable Surface Topography for Programming Unidirectional Liquid Transport. Adv. Funct. Mater. ***29***, 1807858.
15. Lv, P., Zhang, Y.-L., Han, D.-D., and Sun, H. (2021). Directional Droplet Transport on Functional Surfaces with Superwettabilities. Adv. Mater. Interfac. ***8***, 2100043.

16. Thiele, U., John, K., and Bär, M. (2004). Dynamical Model for Chemically Driven Running Droplets. Phys. Rev. Lett. **93**, 027802.
17. Darmanin, T., and Guittard, F. (2014). Recent advances in the potential applications of bio-inspired superhydrophobic materials. J. Mater. Chem. A **2**, 16319–16359.
18. Si, Y., and Dong, Z. (2020). Bioinspired Smart Liquid Directional Transport Control. Langmuir **36**, 667–681.
19. Xia, D., Johnson, L.M., and López, G.P. (2012). Anisotropic Wetting Surfaces with One-Dimesional and Directional Structures: Fabrication Approaches, Wetting Properties and Potential Applications. Adv. Mater. **24**, 1287–1302.
20. Parker, A.R., and Lawrence, C.R. (2001). Water capture by a desert beetle. Nature **414**, 33–34.
21. Yu, Z., Yun, F.F., Wang, Y., et al. (2017). Desert Beetle-Inspired Superwettable Patterned Surfaces for Water Harvesting. Small **13**, 1701403.
22. Zheng, Y., Bai, H., Huang, Z., et al. (2010). Directional water collection on wetted spider silk. Nature **463**, 640–643.
23. Ju, J., Bai, H., Zheng, Y., et al. (2012). A multi-structural and multi-functional integrated fog collection system in cactus. Nat. Commun. **3**, 1247.
24. Luo, C. (2015). Theoretical Exploration of Barrel-Shaped Drops on Cactus Spines. Langmuir **31**, 11809–11813.
25. Chen, H., Zhang, P., Zhang, L., et al. (2016). Continuous directional water transport on the peristome surface of Nepenthes alata. Nature **532**, 85–89.
26. Bohn, H.F., and Federle, W. (2004). Insect aquaplaning: Nepenthes pitcher plants capture prey with the peristome, a fully wettable water-lubricated anisotropic surface. Proc. Natl. Acad. Sci. USA **101**, 14138–14143.
27. Chen, H., Ran, T., Gan, Y., et al. (2018). Ultrafast water harvesting and transport in hierarchical microchannels. Nat. Mater. **17**, 935–942.
28. Gau, H., Herminghaus, S., Lenz, P., and Lipowsky, R. (1999). Liquid morphologies on structured surfaces: from microchannels to microchips. Science **283**, 46–49.
29. Yang, J.-T., Yang, Z.-H., Chen, C.-Y., and Yao, D.J. (2008). Conversion of Surface Energy and Manipulation of a Single Droplet across Micropatterned Surfaces. Langmuir **24**, 9889–9897.
30. Reyssat, M., Pardo, F., and Quéré, D. (2009). Drops onto gradients of texture. Europhys. Lett. **87**, 36003.
31. Élise, L., and Quéré, D. (2004). Drops on a conical wire. J. Fluid Mech. **510**, 29–45.
32. Li, C., Wu, L., Yu, C., et al. (2017). Peristome-Mimetic Curved Surface for Spontaneous and Directional Separation of Micro Water-in-Oil Drops. Angew. Chem. Int. Ed. **56**, 13623–13628.
33. Sun, S., Miao, J., Tan, R., et al. (2023). Asymmetric Soft-Structure Functional Surface for Intelligent Liquids' Distinction, Transportation, and Reaction Mixer. Adv. Funct. Mater. **33**, 2209769.
34. Li, H., Shkolyar, E., Wang, J., et al. (2020). SLIPS-LAB-A bioinspired bioanalysis system for metabolic evaluation of urinary stone disease. Sci. Adv. **6**, eaba8535.
35. Hou, L., Wang, N., Yu, L.-J., et al. (2023). High-Performance Janus Solar Evaporator for Water Purification with Broad Spectrum Absorption and Ultralow Heat Loss. ACS Energy Lett. **8**, 553–564.
36. Hu, R., Wang, N., Hou, L., et al. (2022). Bilayer Nanoporous Polyethylene Membrane with Anisotropic Wettability for Rapid Water Transportation/Evaporation and Radiative Cooling. ACS Appl. Mater. Interfaces **14**, 9833–9843.
37. Liimatainen, V., Vuckovac, M., Jokinen, V., et al. (2017). Mapping microscale wetting variations on biological and synthetic water-repellent surfaces. Nat. Commun. **8**, 1798.
38. Schmüser, L., Zhang, W., Marx, M.T., et al. (2020). Role of Surface Chemistry in the Superhydrophobicity of the Springtail Orchesella cincta (Insecta:Collembola). ACS Appl. Mater. Interfaces **12**, 12294–12304.
39. Malinowski, R., Parkin, I.P., and Volpe, G. (2020). Advances towards programmable droplet transport on solid surfaces and its applications. Chem. Soc. Rev. **49**, 7879–7892.
40. Pan, Z., Pitt, W.G., Zhang, Y., et al. (2016). The upside-down water collection system of Syntrichia caninervis. Nat. Plants **2**, 16076.
41. Chen, D., Niu, S., Zhang, J., et al. (2018). Superfast Liquid Transfer Strategy Through Sliding on a Liquid Membrane Inspired from Scorpion Setae. Adv. Mater. Interfac. **5**, 1800802.
42. Prakash, M., Quéré, D., and Bush, J.W.M. (2008). Surface tension transport of prey by feeding shorebirds: the capillary ratchet. Science **320**, 931–934.
43. Zheng, Y., Gao, X., and Jiang, L. (2007). Directional adhesion of superhydrophobic butterfly wings. Soft Matter **3**, 178–182.
44. Liu, C., Ju, J., Zheng, Y., and Jiang, L. (2014). Asymmetric ratchet effect for directional transport of fog drops on static and dynamic butterfly wings. ACS Nano **8**, 1321–1329.
45. Guadarrama-Cetina, J., Mongruel, A., Medici, M.G., et al. (2014). Dew condensation on desert beetle skin. Eur. Phys. J. E **37**, 109.
46. Feng, S., Zhu, P., Zheng, H., et al. (2021). Three-dimensional capillary ratchet-induced liquid directional steering. Science **373**, 1344–1348.
47. Comanns, P., Buchberger, G., Buchsbaum, A., et al. (2015). Directional, passive liquid transport: the Texas horned lizard as a model for a biomimetic 'liquid diode'. J. R. Soc. Interface **12**, 20150415.
48. Andrews, H.G., Eccles, E.A., Schofield, W.C.E., and Badyal, J.P.S. (2011). Three-dimensional hierarchical structures for fog harvesting. Langmuir **27**, 3798–3802.
49. Tracy, C.R., Laurence, N., and Christian, K.A. (2011). Condensation onto the Skin as a Means for Water Gain by Tree Frogs in Tropical Australia. Am. Nat. **178**, 553–558.
50. Xue, Y., Wang, T., Shi, W., et al. (2014). Water collection abilities of green bristlegrass bristle. RSC Adv. **4**, 40837–40840.
51. Ma, X., Cao, M., Teng, C., et al. (2015). Bio-inspired humidity responsive switch for directional water droplet delivery. J. Mater. Chem. A **3**, 15540–15545.
52. Ebner, M., Miranda, T., and Roth-Nebelsick, A. (2011). Efficient fog harvesting by Stipagrostis sabulicola (Namib dune bushman grass). J. Arid Environ. **75**, 524–531.
53. Abbas, A., Zhang, C., Asad, M., et al. (2022). Recent Developments in Artificial Super-Wettable Surfaces Based on Bioinspired Polymeric Materials for Biomedical Applications. Polymers **14**, 238.
54. Chaudhury, M.K., and Whitesides, G.M. (1992). How to make water run uphill. Science **256**, 1539–1541.
55. Liu, C., Sun, J., Li, J., et al. (2017). Long-range spontaneous droplet self-propulsion on wettability gradient surfaces. Sci. Rep. **7**, 7552.
56. Style, R.W., Che, Y., Park, S.J., et al. (2013). Patterning droplets with durotaxis. Proc. Natl. Acad. Sci. USA **110**, 12541–12544.
57. Malvadkar, N.A., Hancock, M.J., Sekeroglu, K., et al. (2010). An engineered anisotropic nanofilm with unidirectional wetting properties. Nat. Mater. **9**, 1023–1028.
58. Chu, K.-H., Xiao, R., and Wang, E.N. (2010). Uni-directional liquid spreading on asymmetric nanostructured surfaces. Nat. Mater. **9**, 413–417.
59. Lagubeau, G., Le Merrer, M., Clanet, C., and Quéré, D. (2011). Leidenfrost on a ratchet. Nat. Phys. **7**, 395–398.
60. Feng, S., Wang, Q., Xing, Y., et al. (2020). Continuous Directional Water Transport on Integrating Tapered Surfaces. Adv. Mater. Interfac. **7**, 2000081.
61. Ju, J., Xiao, K., Yao, X., et al. (2013). Bioinspired conical copper wire with gradient wettability for continuous and efficient fog collection. Adv. Mater. **25**, 5937–5942.
62. Luo, C., Heng, X., and Xiang, M. (2014). Behavior of a liquid drop between two nonparallel plates. Langmuir **30**, 8373–8380.
63. Xu, W., Lan, Z., Peng, B., et al. (2016). Directional Movement of Droplets in Grooves: Suspended or Immersed? Sci. Rep. **6**, 18836.
64. Hou, L., Wang, N., Wu, J., et al. (2018). Bioinspired Superwettability Electrospun Micro/Nanofibers and Their Applications. Adv. Funct. Mater. **28**, 1801114.
65. Antonietti, M., Henke, S., and Thünemann, A. (1996). Highly ordered materials with ultra-low surface energies: Polyelectrolyte-surfactant, complexes with fluorinated surfactants. Adv. Mater. **8**, 41–45.
66. Hernández, S.C., Bennett, C.J.C., Junkermeier, C.E., et al. (2013). Chemical Gradients on Graphene To Drive Droplet Motion. ACS Nano **7**, 4746–4755.
67. Mazaltarim, A.J., and Morin, S.A. (2022). Programmable Droplet Transport Using Mechanically Adaptive Chemical Gradients with Anisotropic Microtopography. Adv. Intell. Syst. **4**, 2100207.
68. Mazaltarim, A.J., Bowen, J.J., Taylor, J.M., and Morin, S.A. (2021). Dynamic manipulation of droplets using mechanically tunable microtextured chemical gradients. Nat. Commun. **12**, 3114.
69. Rykaczewski, K., Osborn, W.A., Chinn, J., et al. (2012). How nanorough is rough enough to make a surface superhydrophobic during water condensation? Soft Matter **8**, 8786.
70. Schutzius, T.M., Jung, S., Maitra, T., et al. (2015). Spontaneous droplet trampolining on rigid superhydrophobic surfaces. Nature **527**, 82–85.
71. Lafuma, A., and Quéré, D. (2003). Superhydrophobic states. Nat. Mater. **2**, 457–460.
72. Wang, S., and Jiang, L. (2007). Definition of Superhydrophobic States. Adv. Mater. **19**, 3423–3424.
73. Ju, J., Zheng, Y., and Jiang, L. (2014). Bioinspired one-dimensional materials for directional liquid transport. Acc. Chem. Res. **47**, 2342–2352.
74. Lee, S.-W., and Laibinis, P.E. (2000). Directed Movement of Liquids on Patterned Surfaces Using Noncovalent Molecular Adsorption. J. Am. Chem. Soc. **122**, 5395–5396.
75. Choi, S.-H., and Zhang Newby, B.-m. (2003). Micrometer-Scaled Gradient Surfaces Generated Using Contact Printing of Octadecyltrichlorosilane. Langmuir **19**, 7427–7435.
76. Gallardo, B.S., Gupta, V.K., Eagerton, F.D., et al. (1999). Electrochemical Principles for Active Control of Liquids on Submillimeter Scales. Science **283**, 57–60.
77. 't Mannetje, D., Ghosh, S., Lagraauw, R., et al. (2014). Trapping of drops by wetting defects. Nat. Commun. **5**, 3559.
78. Li, J., Ha, N.S., Liu, T.L., et al. (2019). Ionic-surfactant-mediated electro-dewetting for digital microfluidics. Nature **572**, 507–510.
79. Sun, Q., Wang, D., Li, Y., et al. (2019). Surface charge printing for programmed droplet transport. Nat. Mater. **18**, 936–941.
80. Guo, T., Che, P., Heng, L., et al. (2016). Anisotropic Slippery Surfaces: Electric-Driven Smart Control of a Drop's Slide. Adv. Mater. **28**, 6999–7007.
81. Wang, J., Sun, L., Zou, M., et al. (2017). Bioinspired shape-memory graphene film with tunable wettability. Sci. Adv. **3**, e1700004.
82. Ichimura, K., Oh, S.-K., and Nakagawa, M. (2000). Light-driven motion of liquids on a photoresponsive surface. Science **288**, 1624–1626.
83. Lv, J.-a., Liu, Y., Wei, J., et al. (2016). Photocontrol of fluid slugs in liquid crystal polymer microactuators. Nature **537**, 179–184.
84. Brochard, F. (1989). Motions of droplets on solid surfaces induced by chemical or thermal gradients. Langmuir **5**, 432–438.
85. Darhuber, A.A., Valentino, J.P., Troian, S.M., et al. (2003). Thermocapillary actuation of droplets on chemically patterned surfaces by programmable microheater arrays. J. Microelectromech. Syst. **12**, 873–879.
86. Daniel, S., Chaudhury, M.K., and Chen, J.C. (2001). Fast drop movements resulting from the phase change on a gradient surface. Science **291**, 633–636.
87. Liu, C., Sun, J., Zhuang, Y., et al. (2018). Self-propelled droplet-based electricity generation. Nanoscale **10**, 23164–23169.
88. Chai, H., Tian, Y., Yu, S., et al. (2020). Large-Range, Reversible Directional Spreading of Droplet on a Double-Gradient Wrinkled Surface Adjusted Under Mechanical Strain. Adv. Mater. Interfac. **7**, 1901980.

89. Style, R.W., Hyland, C., Boltyanskiy, R., et al. (2013). Surface tension and contact with soft elastic solids. Nat. Commun. ***4***, 2728.
90. Theodorakis, P.E., Egorov, S.A., and Milchev, A. (2017). Stiffness-guided motion of a droplet on a solid substrate. J. Chem. Phys. ***146***, 244705.
91. Style, R.W., Jagota, A., Hui, C.-Y., and Dufresne, E.R. (2017). Elastocapillarity: Surface Tension and the Mechanics of Soft Solids. Annu. Rev. Condens. Matter Phys. ***8***, 99–118.
92. Discher, D.E., Janmey, P., and Wang, Y.L. (2005). Tissue cells feel and respond to the stiffness of their substrate. Science ***310***, 1139–1143.
93. Liu, Q., Zhang, J., Sun, P., et al. (2023). Achieving ultralong directional liquid transportation spontaneously with a high velocity. J. Mater. Chem. A ***11***, 10164–10173.
94. Ghosh, A., Ganguly, R., Schutzius, T.M., et al. (2014). Wettability patterning for high-rate, pumpless fluid transport on open, non-planar microfluidic platforms. Lab Chip ***14***, 1538–1550.
95. Rhee, D., Lee, W.K., and Odom, T.W. (2017). Crack-Free, Soft Wrinkles Enable Switchable Anisotropic Wetting. Angew. Chem. Int. Ed. ***56***, 6523–6527.
96. Quéré, D. (2008). Wetting and Roughness. Annu. Rev. Mater. Res. ***38***, 71–99.
97. Semprebon, C., McHale, G., and Kusumaatmaja, H. (2016). Apparent contact angle and contact angle hysteresis on liquid infused surfaces. Soft Matter ***13***, 101–110.
98. Tuteja, A., Choi, W., Ma, M., et al. (2007). Designing superoleophobic surfaces. Science ***318***, 1618–1622.
99. Butt, H.-J., Liu, J., Koynov, K., et al. (2022). Contact angle hysteresis. Curr. Opin. Colloid. ***59***, 101574.
100. Chu, K.-H., Xiao, R., and Wang, E.N. (2008). Directional Liquid Spreading on Asymmetric Nanostructured Surfaces (APS Division of Fluid Dynamics Meeting Abstracts).
101. Liu, C., Ju, J., Ma, J., Zheng, Y., and Jiang, L. (2014). Directional Drop Transport Achieved on High-Temperature Anisotropic Wetting Surfaces. Adv. Mater. ***26***, 6086–6091.
102. Agapov, R.L., Boreyko, J.B., Briggs, D.P., et al. (2014). Asymmetric Wettability of Nanostructures Directs Leidenfrost Droplets. ACS Nano ***8***, 860–867.
103. Si, Y., Wang, T., Li, C., et al. (2018). Liquids Unidirectional Transport on Dual-Scale Arrays. ACS Nano ***12***, 9214–9222.
104. Würger, A. (2011). Leidenfrost gas ratchets driven by thermal creep. Phys. Rev. Lett. ***107***, 164502.
105. Linke, H., Alemán, B.J., Melling, L.D., et al. (2006). Self-propelled Leidenfrost droplets. Phys. Rev. Lett. ***96***, 154502.
106. Zhang, S., Huang, J., Chen, Z., and Lai, Y. (2017). Bioinspired special wettability surfaces: from fundamental research to water harvesting applications. Small ***13***, 1602992.
107. Zhu, H., Guo, Z., and Liu, W. (2016). Biomimetic water-collecting materials inspired by nature. Chem. Commun. ***52***, 3863–3879.
108. Wang, P., Bian, R., Meng, Q., et al. (2017). Bioinspired Dynamic Wetting on Multiple Fibers. Adv. Mater. ***29***, 1703042.
109. Launay, G., Sadullah, M.S., McHale, G., et al. (2020). Self-propelled droplet transport on shaped-liquid surfaces. Sci. Rep. ***10***, 14987.
110. Liu, Z., Liu, H., Li, W., and Song, J. (2022). Optimization of bioinspired surfaces with enhanced water transportation capacity. Chem. Eng. J. ***433***, 134568.
111. Li, J., Li, J., Sun, J., et al. (2019). Biological and Engineered Topological Droplet Rectifiers. Adv. Mater. ***31***, 1806501.
112. Shi, Z., Tang, Z., Xu, B., et al. (2022). Bioinspired directional liquid transport induced by the corner effect. Nano Res. ***16***, 3913–3923.
113. Duprat, C., Protière, S., Beebe, A.Y., and Stone, H.A. (2012). Wetting of flexible fibre arrays. Nature ***482***, 510–513.
114. Lv, C., Chen, C., Chuang, Y.-C., et al. (2014). Substrate Curvature Gradient Drives Rapid Droplet Motion. Phys. Rev. Lett. ***113***, 026101.
115. Liang, Y.-E., Tsao, H.-K., and Sheng, Y.-J. (2015). Drops on Hydrophilic Conical Fibers: Gravity Effect and Coexistent States. Langmuir ***31***, 1704–1710.
116. Hou, Y., Gao, L., Feng, S., et al. (2013). Temperature-triggered directional motion of tiny water droplets on bioinspired fibers in humidity. Chem. Commun. ***49***, 5253–5255.
117. Mahmood, A., Chen, S., Chen, C., et al. (2018). Directional Motion of Water Droplet on Nanocone Surface Driven by Curvature Gradient: A Molecular Dynamics Simulation Study. J. Phys. Chem. C ***122***, 14937–14944.
118. Hanumanthu, R., and Stebe, K.J. (2006). Equilibrium shapes and locations of axisymmetric, liquid drops on conical, solid surfaces. Colloid. Surface. ***282–283***, 227–239.
119. Fisher, L.R., Gamble, R.A., and Middlehurst, J. (1981). The Kelvin equation and the capillary condensation of water. Nature ***290***, 575–576.
120. Hu, R., Wang, N., Hou, L., et al. (2019). A bioinspired hybrid membrane with wettability and topology anisotropy for highly efficient fog collection. J. Mater. Chem. A ***7***, 124–132.
121. Zou, J., Wang, P.F., Zhang, T.R., et al. (2011). Experimental study of a drop bouncing on a liquid surface. Phys. Fluids ***23***, 044101.
122. Shi, Y., Ilic, O., Atwater, H.A., and Greer, J.R. (2021). All-day fresh water harvesting by microstructured hydrogel membranes. Nat. Commun. ***12***, 2797.
123. Bai, H., Ju, J., Sun, R., et al. (2011). Controlled Fabrication and Water Collection Ability of Bioinspired Artificial Spider Silks. Adv. Mater. ***23***, 3708–3711.
124. Dong, H., Zheng, Y., Wang, N., et al. (2016). Highly efficient fog collection unit by integrating artificial spider silks. Adv. Mater. Interfac. ***3***, 1500831.
125. Bai, H., Sun, R., Ju, J., et al. (2011). Large-Scale Fabrication of Bioinspired Fibers for Directional Water Collection. Small ***7***, 3429–3433.
126. Xue, Y., Chen, Y., Wang, T., et al. (2014). Directional size-triggered microdroplet target transport on gradient-step fibers. J. Mater. Chem. A ***2***, 7156–7160.
127. Dong, H., Wang, N., Wang, L., et al. (2012). Bioinspired electrospun knotted microfibers for fog harvesting. ChemPhysChem ***13***, 1153–1156.
128. Tian, X., Bai, H., Zheng, Y., et al. (2011). Bio-inspired heterostructured bead-on-string fibers that respond to environmental wetting. Adv. Funct. Mater. ***21***, 1398–1402.
129. Du, M., Zhao, Y., Tian, Y., et al. (2016). Electrospun multiscale structured membrane for efficient water collection and directional transport. Small ***12***, 1000–1005.
130. Tian, Y., Zhu, P., Tang, X., et al. (2017). Large-scale water collection of bioinspired cavity-microfibers. Nat. Commun. ***8***, 1080.
131. He, X.H., Wang, W., Liu, Y.M., et al. (2015). Microfluidic Fabrication of Bio-Inspired Microfibers with Controllable Magnetic Spindle-Knots for 3D Assembly and Water Collection. ACS Appl. Mater. Interfaces ***7***, 17471–17481.
132. Liu, Y., Yang, N., Li, X., et al. (2020). Water Harvesting of Bioinspired Microfibers with Rough Spindle-Knots from Microfluidics. Small ***16***, 1901819.
133. Dai, H., Dong, Z., and Jiang, L. (2020). Directional liquid dynamics of interfaces with superwettability. Sci. Adv. ***6***, eabb5528.
134. Wong, T.-S., Kang, S.H., Tang, S.K.Y., et al. (2011). Bioinspired self-repairing slippery surfaces with pressure-stable omniphobicity. Nature ***477***, 443–447.
135. Wang, Z., Liu, Y., Guo, P., et al. (2018). Photoelectric Synergetic Responsive Slippery Surfaces Based on Tailored Anisotropic Films Generated by Interfacial Directional Freezing. Adv. Funct. Mater. ***28***, 1801310.
136. Wang, J., Gao, W., Zhang, H., et al. (2018). Programmable wettability on photocontrolled graphene film. Sci. Adv. ***4***, eaat7392.
137. Sun, L., Bian, F., Wang, Y., et al. (2020). Bioinspired programmable wettability arrays for droplets manipulation. Proc. Natl. Acad. Sci. USA ***117***, 4527–4532.
138. Mugele, F. (2019). Droplet motion electrically controlled. Nature ***572***, 445–446.
139. Li, J., Han, X., Li, W., et al. (2023). Nature-inspired reentrant surfaces. Prog. Mater. Sci. ***133***, 101064.
140. Lee, M., Oh, J., Lim, H., and Lee, J. (2021). Enhanced Liquid Transport on a Highly Scalable, Cost-Effective, and Flexible 3D Topological Liquid Capillary Diode. Adv. Funct. Mater. ***31***, 2011288.
141. Chen, H., Zhang, L., Zhang, P., et al. (2017). A novel bioinspired continuous unidirectional liquid spreading surface structure from the peristome surface of Nepenthes alata. Small ***13***, 1601676.
142. Zhang, P., Zhang, L., Chen, H., et al. (2017). Surfaces inspired by the nepenthes peristome for unidirectional liquid transport. Adv. Mater. ***29***, 1702995.
143. Li, C., Li, N., Zhang, X., et al. (2016). Uni-Directional Transportation on Peristome-Mimetic Surfaces for Completely Wetting Liquids. Angew. Chem. Int. Ed. ***55***, 14988–14992.
144. Li, J., Zhou, X., Li, J., et al. (2017). Topological liquid diode. Sci. Adv. ***3***, eaao3530.
145. Yu, C., Li, C., Gao, C., et al. (2018). Time-Dependent Liquid Transport on a Biomimetic Topological Surface. ACS Nano ***12***, 5149–5157.
146. Li, C., Dai, H., Gao, C., et al. (2019). Bioinspired inner microstructured tube controlled capillary rise. Proc. Natl. Acad. Sci. USA ***116***, 12704–12709.
147. Xie, D., Sun, Y., Wu, Y., et al. (2023). Engineered Switchable-Wettability Surfaces for Multi-Path Directional Transportation of Droplets and Subaqueous Bubbles. Adv. Mater. ***35***, 2208645.
148. Kong, T., Stone, H.A., Wang, L., and Shum, H.C. (2018). Dynamic regimes of electrified liquid filaments. Proc. Natl. Acad. Sci. USA ***115***, 6159–6164.
149. Tabassian, R., Oh, J.-H., Kim, S., et al. (2016). Graphene-coated meshes for electroactive flow control devices utilizing two antagonistic functions of repellency and permeability. Nat. Commun. ***7***, 13345.
150. Yan, Y., Guo, Z., Zhang, X., et al. (2018). Electrowetting-Induced Stiction Switch of a Microstructured Wire Surface for Unidirectional Droplet and Bubble Motion. Adv. Funct. Mater. ***28***, 1800775.
151. Lin, Z.-H., Cheng, G., Lin, L., et al. (2013). Water-Solid Surface Contact Electrification and its Use for Harvesting Liquid-Wave Energy. Angew. Chem. Int. Ed. ***52***, 12545–12549.
152. McCarty, L.S., and Whitesides, G.M. (2008). Electrostatic charging due to separation of ions at interfaces: Contact electrification of ionic electrets. Angew. Chem. Int. Ed. ***47***, 2188–2207.
153. Scatena, L.F., Brown, M.G., and Richmond, G.L. (2001). Water at hydrophobic surfaces: Weak hydrogen bonding and strong orientation effects. Science ***292***, 908–912.
154. Qi, X.-R., Liu, Y., Ma, L.-L., et al. (2022). Delicate synthesis of quasi-inverse opal structural $Na_3V_2(PO_4)_3$/N-C and $Na_4MnV(PO_4)_3$/N-C as cathode for high-rate sodium-ion batteries. Rare Met. ***41***, 1637–1646.
155. Kwon, G., Panchanathan, D., Mahmoudi, S.R., et al. (2017). Visible light guided manipulation of liquid wettability on photoresponsive surfaces. Nat. Commun. ***8***, 14968.
156. Yilmaz, M., Kuloglu, H.B., Erdogan, H., et al. (2015). Light-Driven Unidirectional Liquid Motion on Anisotropic Gold Nanorod Arrays. Adv. Mater. Interfac. ***2***, 1500226.
157. Xiao, Y., Zarghami, S., Wagner, K., et al. (2018). Moving Droplets in 3D Using Light. Adv. Mater. ***30***, 1801821.
158. An, S., Zhu, M., Gu, K., et al. (2020). Light-driven motion of water droplets with directional control on nanostructured surfaces. Nanoscale ***12***, 4295–4301.
159. Wang, F., Liu, M., Liu, C., et al. (2022). Light-induced charged slippery surfaces. Sci. Adv. ***8***, eabp9369.
160. Kobatake, S., Takami, S., Muto, H., et al. (2007). Rapid and reversible shape changes of molecular crystals on photoirradiation. Nature ***446***, 778–781.
161. Xia, F., and Jiang, L. (2008). Bio-Inspired, Smart, Multiscale Interfacial Materials. Adv. Mater. ***20***, 2842–2858.
162. Manabe, K., Saito, K., Nakano, M., et al. (2022). Light-Driven Liquid Conveyors: Manipulating Liquid Mobility and Transporting Solids on Demand. ACS Nano ***16***, 16353–16362.
163. Tian, D., Zhang, N., Zheng, X., et al. (2016). Fast Responsive and Controllable Liquid Transport on a Magnetic Fluid/Nanoarray Composite Interface. ACS Nano ***10***, 6220–6226.

164. Ben, S., Zhou, T., Ma, H., et al. (2019). Multifunctional Magnetocontrollable Superwettable-Microcilia Surface for Directional Droplet Manipulation. Adv. Sci. ***6***, 1900834.
165. Zhang, Y., and Wang, T.-H. (2013). Full-Range Magnetic Manipulation of Droplets via Surface Energy Traps Enables Complex Bioassays. Adv. Mater. ***25***, 2903–2908.
166. Lei, W., Hou, G., Liu, M., et al. (2018). High-speed transport of liquid droplets in magnetic tubular microactuators. Sci. Adv. ***4***, eaau8767.
167. Si, Y., Hu, J., and Dong, Z. (2021). Bioinspired magnetically driven liquid manipulation as microrobot. Cell Reports Physical Science ***2***, 100439.
168. Timonen, J.V.I., Latikka, M., Leibler, L., et al. (2013). Switchable Static and Dynamic Self-Assembly of Magnetic Droplets on Superhydrophobic Surfaces. Science ***341***, 253–257.
169. Yang, C., and Li, G. (2017). A novel magnet-actuated droplet manipulation platform using a floating ferrofluid film. Sci. Rep. ***7***, 15705.
170. Feng, W., Ueda, E., and Levkin, P.A. (2018). Droplet Microarrays: From Surface Patterning to High-Throughput Applications. Adv. Mater. ***30***, 1706111.
171. Yakhshi-Tafti, E., Cho, H.J., and Kumar, R. (2010). Droplet actuation on a liquid layer due to thermocapillary motion: Shape effect. Appl. Phys. Lett. ***96***, 264101.
172. Cira, N.J., Benusiglio, A., and Prakash, M. (2015). Vapour-mediated sensing and motility in two-component droplets. Nature ***519***, 446–450.
173. Li, C., Yu, C., Hao, D., et al. (2018). Smart Liquid Transport on Dual Biomimetic Surface via Temperature Fluctuation Control. Adv. Funct. Mater. ***28***, 1707490.
174. Li, J., Hou, Y., Liu, Y., et al. (2016). Directional transport of high-temperature Janus droplets mediated by structural topography. Nat. Phys. ***12***, 606–612.
175. Liu, M., Li, J., Zhou, X., et al. (2020). Inhibiting Random Droplet Motion on Hot Surfaces by Engineering Symmetry-Breaking Janus-Mushroom Structure. Adv. Mater. ***32***, 1907999.
176. Li, C., Li, M., Ni, Z., et al. (2021). Stimuli-responsive surfaces for switchable wettability and adhesion. J. R. Soc. Interface ***18***, 20210162.
177. Liu, C., Sun, Y., Huanng, J., et al. (2021). External-field-induced directional droplet transport: A review. Adv. Colloid Interface Sci. ***295***, 102502.
178. Yang, C., Zeng, Q., Huang, J., and Guo, Z. (2022). Droplet manipulation on superhydrophobic surfaces based on external stimulation: A review. Adv. Colloid Interface Sci. ***306***, 102724.
179. Li, C., Yu, C., Zhou, S., et al. (2020). Liquid harvesting and transport on multiscaled curvatures. Proc. Natl. Acad. Sci. USA ***117***, 23436–23442.
180. Yu, C., Zhang, L., Ru, Y., et al. (2018). Drop Cargo Transfer via Unidirectional Lubricant Spreading on Peristome-Mimetic Surface. ACS Nano ***12***, 11307–11315.
181. Zhang, Y., Li, J., Xiang, L., et al. (2022). A Biocompatible Vibration-Actuated Omni-Droplets Rectifier with Large Volume Range Fabricated by Femtosecond Laser. Adv. Mater. ***34***, 2108567.
182. Lu, H., Shi, W., Guo, Y., et al. (2022). Materials Engineering for Atmospheric Water Harvesting: Progress and Perspectives. Adv. Mater. ***34***, 2110079.
183. Wang, J., Yi, S., Yang, Z., et al. (2020). Laser Direct Structuring of Bioinspired Spine with Backward Microbarbs and Hierarchical Microchannels for Ultrafast Water Transport and Efficient Fog Harvesting. ACS Appl. Mater. Interfaces ***12***, 21080–21087.
184. Zhou, S., Yu, C., Li, C., et al. (2020). Droplets Crawling on Peristome-Mimetic Surfaces. Adv. Funct. Mater. ***30***, 1908066.
185. Xu, Y., Rather, A.M., Yao, Y., et al. (2021). Liquid crystal-based open surface microfluidics manipulate liquid mobility and chemical composition on demand. Sci. Adv. ***7***, eabi7607.
186. Casagrande, C., Fabre, P., Raphaël, E., and Veyssié, M. (1989). "Janus Beads": Realization and Behaviour at Water/Oil Interfaces. Europhys. Lett. ***9***, 251–255.
187. Yan, L., Yang, X., Zhang, Y., et al. (2021). Porous Janus materials with unique asymmetries and functionality. Mater. Today ***51***, 626–647.
188. Cao, M., Xiao, J., Yu, C., et al. (2015). Hydrophobic/Hydrophilic Cooperative Janus System for Enhancement of Fog Collection. Small ***11***, 4379–4384.
189. Wang, X., Huang, Z., Miao, D., et al. (2019). Biomimetic Fibrous Murray Membranes with Ultrafast Water Transport and Evaporation for Smart Moisture-Wicking Fabrics. ACS Nano ***13***, 1060–1070.
190. Hu, L., Gao, S., Zhu, Y., et al. (2015). An ultrathin bilayer membrane with asymmetric wettability for pressure responsive oil/water emulsion separation. J. Mater. Chem. A ***3***, 23477–23482.
191. Zuo, J.-H., Gu, Y.-H., Wei, C., et al. (2020). Janus polyvinylidene fluoride membranes fabricated with thermally induced phase separation and spray-coating technique for the separations of both W/O and O/W emulsions. J. Membr. Sci. ***595***, 117475.
192. Ding, Y., Tu, K., Burgert, I., et al. (2020). Janus wood membranes for autonomous water transport and fog collection. J. Mater. Chem. A ***8***, 22001–22008.
193. Wang, Y., Xia, G., Yu, H., et al. (2021). Mussel-Inspired Design of a Self-Adhesive Agent for Durable Moisture Management and Bacterial Inhibition on PET Fabric. Adv. Mater. ***33***, 2100140.
194. Chew, N.G.P., Zhang, Y., Goh, K., et al. (2019). Hierarchically Structured Janus Membrane Surfaces for Enhanced Membrane Distillation Performance. ACS Appl. Mater. Interfaces ***11***, 25524–25534.
195. Chen, J., Yin, J.L., Li, B., et al. (2020). Janus Evaporators with Self-Recovering Hydrophobicity for Salt-Rejecting Interfacial Solar Desalination. ACS Nano ***14***, 17419–17427.
196. Gao, C., Sun, Z., Li, K., et al. (2013). Integrated oil separation and water purification by a double-layer TiO_2-based mesh. Energy Environ. Sci. ***6***, 1147–1151.
197. Pei, C., Peng, Y., Zhang, Y., et al. (2018). An Integrated Janus Mesh: Underwater Bubble Antibuoyancy Unidirectional Penetration. ACS Nano ***12***, 5489–5494.
198. Zhong, L., Feng, J., and Guo, Z. (2019). An alternating nanoscale (hydrophilic–hydrophobic)/hydrophilic Janus cooperative copper mesh fabricated by a simple liquidus modification for efficient fog harvesting. J. Mater. Chem. A ***7***, 8405–8413.
199. Wu, J., Wang, N., Wang, L., et al. (2012). Unidirectional water-penetration composite fibrous film via electrospinning. Soft Matter ***8***, 5996–5999.
200. Wu, J., Zhou, H., Wang, H., et al. (2019). Novel Water Harvesting Fibrous Membranes with Directional Water Transport Capability. Adv. Mater. Interfac. ***6***, 1801529.
201. Dong, Y., Kong, J., Phua, S.L., et al. (2014). Tailoring Surface Hydrophilicity of Porous Electrospun Nanofibers to Enhance Capillary and Push-Pull Effects for Moisture Wicking. ACS Appl. Mater. Interfaces ***6***, 14087–14095.
202. Zhu, Z., Liu, Z., Zhong, L., et al. (2018). Breathable and asymmetrically superwettable Janus membrane with robust oil-fouling resistance for durable membrane distillation. J. Membr. Sci. ***563***, 602–609.
203. Shi, L., Liu, X., Wang, W., et al. (2019). A Self-Pumping Dressing for Draining Excessive Biofluid around Wounds. Adv. Mater. ***31***, 1804187.
204. Hou, L., Wang, N., Man, X., et al. (2019). Interpenetrating Janus Membrane for High Rectification Ratio Liquid Unidirectional Penetration. ACS Nano ***13***, 4124–4132.
205. Jiang, Y., Hou, J., Xu, J., and Shan, B. (2017). Switchable oil/water separation with efficient and robust Janus nanofiber membranes. Carbon ***115***, 477–485.
206. An, Y.-P., Yang, J., Yang, H.-C., et al. (2018). Janus Membranes with Charged Carbon Nanotube Coatings for Deemulsification and Separation of Oil-in-Water Emulsions. ACS Appl. Mater. Interfaces ***10***, 9832–9840.
207. Liu, J., Wang, N., Yu, L.-J., et al. (2017). Bioinspired graphene membrane with temperature tunable channels for water gating and molecular separation. Nat. Commun. ***8***, 2011.
208. Liu, J., Yu, L.-j., Yue, G., et al. (2019). Thermoresponsive Graphene Membranes with Reversible Gating Regularity for Smart Fluid Control. Adv. Funct. Mater. ***29***, 1808501.
209. Liu, Y., Xiao, T., Bao, C., et al. (2018). Fabrication of novel Janus membrane by nonsolvent thermally induced phase separation (NTIPS) for enhanced performance in membrane distillation. J. Membr. Sci. ***563***, 298–308.
210. Song, H.-M., Chen, C., Shui, X.-X., et al. (2019). Asymmetric Janus membranes based on *in situ* mussel-inspired chemistry for efficient oil/water separation. J. Membr. Sci. ***573***, 126–134.
211. Wang, H., Ding, J., Dai, L., et al. (2010). Directional water-transfer through fabrics induced by asymmetric wettability. J. Mater. Chem. ***20***, 7938–7940.
212. Kong, Y., Liu, Y., and Xin, J.H. (2011). Fabrics with self-adaptive wettability controlled by "light-and-dark". J. Mater. Chem. ***21***, 17978–17987.
213. Zhang, D., Liu, J., Chen, B., et al. (2018). A Hydrophilic/Hydrophobic Janus Inverse-Opal Actuator via Gradient Infiltration. ACS Nano ***12***, 12149–12158.
214. Li, C., Li, X., Du, X., et al. (2019). Antiwetting and Antifouling Janus Membrane for Desalination of Saline Oily Wastewater by Membrane Distillation. ACS Appl. Mater. Interfaces ***11***, 18456–18465.
215. Miao, D., Wang, X., Yu, J., and Ding, B. (2021). A Biomimetic Transpiration Textile for Highly Efficient Personal Drying and Cooling. Adv. Funct. Mater. ***31***, 2008705.
216. Li, N., Yu, C., Si, Y., et al. (2018). Janus Gradient Meshes for Continuous Separation and Collection of Flowing Oils under Water. ACS Appl. Mater. Interfaces ***10***, 7504–7511.
217. Yang, J., Li, H.-N., Chen, Z.-X., et al. (2019). Janus membranes with controllable asymmetric configurations for highly efficient separation of oil-in-water emulsions. J. Mater. Chem. A ***7***, 7907–7917.
218. Feng, J., Zhong, L., and Guo, Z. (2020). Sprayed hieratical biomimetic superhydrophilic-superhydrophobic surface for efficient fog harvesting. Chem. Eng. J. ***388***, 124283.
219. Li, Y., Zhang, G., Gao, A., et al. (2019). Robust Graphene/Poly(vinyl alcohol) Janus Aerogels with a Hierarchical Architecture for Highly Efficient Switchable Separation of Oil/Water Emulsions. ACS Appl. Mater. Interfaces ***11***, 36638–36648.
220. Zeng, C., Wang, H., Zhou, H., and Lin, T. (2016). Directional Water Transport Fabrics with Durable Ultra-High One-Way Transport Capacity. Adv. Mater. Interfac. ***3***, 1600036.
221. Wu, Z., Yin, K., Wu, J., et al. (2021). Recent advances in femtosecond laser-structured Janus membranes with asymmetric surface wettability. Nanoscale ***13***, 2209–2226.
222. Yang, S., Yin, K., Wu, J., et al. (2019). Ultrafast nano-structuring of superwetting Ti foam with robust antifouling and stability towards efficient oil-in-water emulsion separation. Nanoscale ***11***, 17607–17614.
223. Wu, D., Zhang, Z., Zhang, Y., et al. (2020). High-Performance Unidirectional Manipulation of Microdroplets by Horizontal Vibration on Femtosecond Laser-Induced Slant Microwall Arrays. Adv. Mater. ***32***, 2005039.
224. Wu, J., Yin, K., Li, M., et al. (2020). Under-oil self-driven and directional transport of water on a femtosecond laser-processed superhydrophilic geometry-gradient structure. Nanoscale ***12***, 4077–4084.
225. Lin, Y., Wang, C., Miao, D., et al. (2022). A Trilayered Composite Fabric with Directional Water Transport and Resistance to Blood Penetration for Medical Protective Clothing. ACS Appl. Mater. Interfaces ***14***, 18944–18953.
226. Zhang, Q., Li, Y., Yan, Y., et al. (2020). Highly Flexible Monolayered Porous Membrane with Superhydrophilicity-Hydrophilicity for Unidirectional Liquid Penetration. ACS Nano ***14***, 7287–7296.
227. Shou, D., and Fan, J. (2018). An All Hydrophilic Fluid Diode for Unidirectional Flow in Porous Systems. Adv. Funct. Mater. ***28***, 1800269.
228. Li, P., Cao, M., Bai, H., et al. (2019). Unidirectional Liquid Manipulation Via an Integrated Mesh with Orthogonal Anisotropic Slippery Tracks. Adv. Funct. Mater. ***29***, 1904446.
229. Dai, B., Li, K., Shi, L., et al. (2019). Bioinspired Janus Textile with Conical Micropores for Human Body Moisture and Thermal Management. Adv. Mater. ***31***, 1904113.
230. Yang, H.-C., Hou, J., Chen, V., and Xu, Z.K. (2016). Janus membranes: exploring duality for advanced separation. Angew. Chem. Int. Ed. ***55***, 13398–13407.
231. Zhao, Y., Wang, H., Zhou, H., and Lin, T. (2017). Directional Fluid Transport in Thin Porous Materials and its Functional Applications. Small ***13***, 1601070.
232. Fu, S., Zhou, H., Wang, H., et al. (2019). Superhydrophilic, Underwater Directional Oil-Transport Fabrics with a Novel Oil Trapping Function. ACS Appl. Mater. Interfaces ***11***, 27402–27409.
233. Xu, W., Hu, X., Zhuang, S., et al. (2018). Flexible and Salt Resistant Janus Absorbers by Electrospinning for Stable and Efficient Solar Desalination. Adv. Energy Mater. ***8***, 1702884.

234. Zhang, X., Fu, Q., Duan, H., et al. (2021). Janus Nanoparticles: From Fabrication to (Bio) Applications. ACS Nano ***15***, 6147–6191.
235. Hou, L., Liu, J., Li, D., et al. (2021). Electrospinning Janus Nanofibrous Membrane for Unidirectional Liquid Penetration and Its Applications. Chem. Res. Chin. Univ. ***37***, 337–354.
236. Wang, H., Zhou, H., Niu, H., et al. (2015). Dual-layer superamphiphobic/superhydrophobic-oleophilic nanofibrous membranes with unidirectional oil-transport ability and strengthened oil-water separation performance. Adv. Mater. Interfac. ***2***, 1400506.
237. Tian, X., Jin, H., Sainio, J., et al. (2014). Droplet and fluid gating by biomimetic Janus membranes. Adv. Funct. Mater. ***24***, 6023–6028.
238. Afsari, M., Shon, H.K., and Tijing, L.D. (2021). Janus membranes for membrane distillation: Recent advances and challenges. Adv. Colloid Interface Sci. ***289***, 102362.
239. Huang, Y.-X., Wang, Z., Jin, J., et al. (2017). Novel Janus membrane for membrane distillation with simultaneous fouling and wetting resistance. Environ. Sci. Technol. ***51***, 13304–13310.
240. Jeppesen, E., Beklioğlu, M., Özkan, K., and Akyürek, Z. (2020). Salinization Increase due to Climate Change Will Have Substantial Negative Effects on Inland Waters: A Call for Multifaceted Research at the Local and Global Scale. Innovation ***1***, 100030.
241. Yao, H., Zhang, P., Yang, C., et al. (2021). Janus-interface engineering boosting solar steam towards high-efficiency water collection. Energy Environ. Sci. ***14***, 5330–5338.
242. Yang, Y., Yang, X., Fu, L., et al. (2018). Two-Dimensional Flexible Bilayer Janus Membrane for Advanced Photothermal Water Desalination. ACS Energy Lett. ***3***, 1165–1171.
243. Chang, Y., Wang, Z., Shi, Y.-E., et al. (2018). Hydrophobic $W_{18}O_{49}$ mesocrystal on hydrophilic PTFE membrane as an efficient solar steam generation device under one sun. J. Mater. Chem. A ***6***, 10939–10946.
244. Liu, Z., Qing, R.-K., Xie, A.-Q., et al. (2021). Self-contained Janus Aerogel with Antifouling and Salt-Rejecting Properties for Stable Solar Evaporation. ACS Appl. Mater. Interfaces ***13***, 18829–18837.
245. Li, H.-N., Liu, Y.-W., Hu, Y.-Q., et al. (2022). Magnetic-controllable Janus fibrous membranes with wind-resistant floatability for airflow-enhanced solar evaporation. J. Polym. Sci. ***60***, 2309–2317.
246. Hu, Y., Ma, H., Wu, M., et al. (2022). A reconfigurable and magnetically responsive assembly for dynamic solar steam generation. Nat. Commun. ***13***, 4335.
247. Han, D.-D., Chen, Z.-D., Li, J.-C., et al. (2020). Airflow Enhanced Solar Evaporation Based on Janus Graphene Membranes with Stable Interfacial Floatability. ACS Appl. Mater. Interfaces ***12***, 25435–25443.
248. Yang, S., Zhu, Z., Wu, Z., et al. (2020). Femtosecond laser rapid fabrication of Janus sweat-permeable fabric for personal cooling. Appl. Phys. Lett. ***117***, 213701.
249. Fu, C., Gu, L., Zeng, Z., and Xue, Q. (2020). Simply Adjusting the Unidirectional Liquid Transport of Scalable Janus Membranes toward Moisture-Wicking Fabric, Rapid Demulsification, and Fast Oil/Water Separation. ACS Appl. Mater. Interfaces ***12***, 51102–51113.
250. Lao, L., Shou, D., Wu, Y.S., and Fan, J.T. (2020). "Skin-like" fabric for personal moisture management. Sci. Adv. ***6***, eaaz0013.
251. Wang, Y., Liang, X., Zhu, H., et al. (2020). Reversible Water Transportation Diode: Temperature-Adaptive Smart Janus Textile for Moisture/Thermal Management. Adv. Funct. Mater. ***30***, 1907851.
252. Miao, D., Cheng, N., Wang, X., et al. (2022). Sandwich-Structured textiles with hierarchically nanofibrous network and Janus wettability for outdoor personal thermal and moisture management. Chem. Eng. J. ***450***, 138012.
253. Yang, W., Gong, W., Hou, C., et al. (2019). All-fiber tribo-ferroelectric synergistic electronics with high thermal-moisture stability and comfortability. Nat. Commun. ***10***, 5541.
254. Lei, M., Qu, X., Liu, H., et al. (2019). Programmable Electrofabrication of Porous Janus Films with Tunable Janus Balance for Anisotropic Cell Guidance and Tissue Regeneration. Adv. Funct. Mater. ***29***, 1900065.
255. Zhang, X., Zhu, Y., Fang, W., et al. (2021). Thin film composite structured Janus membrane for fast gravity-driven separation of a trace of blood. J. Membr. Sci. ***620***, 118853.

ACKNOWLEDGMENTS

This work was supported by the National Natural Science Foundation of China (NSFC) (22105012, 21975007, 22175007, 52172080), Beijing Natural Science Foundation (2232054), the National Natural Science Foundation of China for Outstanding Youth Foundation, the Fundamental Research Funds for the Central Universities, the National Program for Support of Top-notch Young Professionals, the 111 Project (grant no. B14009), and the open project of the Key Laboratory of Photochemical Conversion and Optoelectronic Materials, Technical Institute of Physics and Chemistry, Chinese Academy of Sciences.

AUTHOR CONTRIBUTIONS

L.L.H., N.W., and Y.Z. conceived and wrote this article. L.L.H. organized the logical structure of the article and created the figures. Z.M.C., X.F.L., X.R.G., and R.J.H. collected the literature resources. All authors participated in the discussions and provided comments on the manuscript.

DECLARATION OF INTERESTS

The authors declare no competing interests.

LEAD CONTACT WEBSITE

https://m.x-mol.com/groups/zhao